Transpressional tectonics along the Karakoram fault zone, northern Ladakh: constraints on Tibetan extrusion

M. P. SEARLE[1], R. F. WEINBERG[2,1] & W. J. DUNLAP[2]

[1]*Department of Earth Sciences, Oxford University, Parks Road, Oxford OX1 3PR, UK*

[2]*Research School of Earth Sciences, Australian National University, Canberra, A.C.T. 0200, Australia*

Abstract: The Tibetan plateau north of the Himalaya has approximately double normal crustal thickness (60–75 km) and has been homogeneously shortened since the India–Asia collision at 60–50 Ma ago, yet, with minimal erosion rates, has almost no middle or deep crustal rocks exposed at the surface. In the Karakoram range, west of Tibet, early Tertiary crustal thickening and regional metamorphism resulted in Miocene crustal melting producing the Baltoro monzogranite–leucogranite batholith. Late Tertiary transpression along the western margin of the Tibetan plateau, caused by the continued northward penetration of India into Asia, led to exhumation of migmatites in the Pangong range and Baltoro-type granites along the Karakoram fault. Detailed studies of the Karakoram fault zone in northern Ladakh, India, show that Baltoro-type two-mica ± garnet leucogranites, intruded 21–18.0 Ma ago, have been offset a maximum of 150 km right-laterally. Average slip rates since 18.0 ± 0.6 Ma (2σ) are 8.3 mm/a. $^{40}Ar/^{39}Ar$ mica cooling ages are 11.3 Ma on both sides of the main (southwestern) strand of the fault, suggesting that most of the exhumation of the Pangong migmatites and leucogranites must have occurred between 18.0 and 11.3 Ma. During this time, at slip rates of 8.3 mm/a the rocks would have moved horizontally right-laterally for *c.* 56 km and been exhumed by *c.* 20 km vertically during transpression, using the measured 20° plunge of lineations.

The high exhumation rate (3.0 mm/a) and amount of erosion (20 km) inferred between 18.0 and 11.3 Ma may also reflect the partitioning between an early transpressional strain associated with crustal thickening and exhumation of the Pangong deep crustal migmatites and leucogranites, and a later dominantly dextral strike-slip phase of fault motion along the central part of the Karakoram fault from *c.* 11 to 0 Ma. This timing may also coincide with the initiation of the N–S aligned normal faults and E–W extension in southern Tibet. We suggest that the relatively minor dextral offset (150 km) and the young age of initiation on this bounding fault do not support the model of large-scale extrusion of Tibetan crust, but they suggest instead that deformation of Tibet was taken up predominantly by crustal thickening.

One of the major questions concerning the continental tectonics of Asia is to what extent has the double normal thickness crust of the Tibetan plateau region been extruded eastwards, out of the way of the Indian indentor. The pattern of active strike-slip faults across Asia (Fig. 1) led Molnar & Tapponnier (1975) to suggest that Tibet was being forced eastwards out of the way of the northward indenting Indian crust. The continental extrusion hypothesis has subsequently been greatly expanded upon by Tapponnier & Molnar (1976, 1977), Tapponnier *et al.* (1982, 1986), Peltzer & Tapponnier (1988), Armijo *et al.* (1989), Peltzer *et al.* (1989) and Avouac & Tapponnier (1993). The boundaries of the extruding crust have been defined as the 2500 km long sinistral Altyn Tagh fault along the northern boundary of Tibet (Peltzer & Tapponnier 1988; Peltzer *et al.* 1989; Meyer *et al.* 1996) and the 1000 km long dextral Karakoram fault along the southwestern margin of Tibet (Fig. 1). The Karakoram fault actually merges with the Indus suture zone in the region of Mt Kailas, although most proponents of the continental extrusion hypothesis link the Karakoram fault in the west to the Jiali fault in southeast Tibet via a series of NW–SE aligned small-scale strike-slip faults across southern Tibet (Armijo *et al.* 1989; Avouac & Tapponnier 1993).

Estimates of geological offsets by Peltzer & Tapponnier (1988, plate 2, p. 15 358) suggested *c.* 500 km of left-lateral offset along the Altyn Tagh fault and *c.* 1000 km of right-lateral offset along the Karakoram fault. Holocene slip rates along the Altyn Tagh fault were estimated as being *c.* 20 mm/a in the west, 30 mm/a in the central part and 4 ± 2 mm/a in the far east (Avouac & Tapponnier 1993; Meyer *et al.* 1996). For the Karakoram fault, Holocene slip rates of *c.* 32 mm/a were proposed by Avouac & Tapponnier

SEARLE, M. P., WEINBERG, R. F. & DUNLAP, W. J. 1998. Transpressional tectonics along the Karakoram fault zone, northern Ladakh: constraints on Tibetan extrusion. *In:* HOLDSWORTH, R. E., STRACHAN, R. A. & DEWEY, J. F. (eds) 1998. *Continental Transpressional and Transtensional Tectonics*. Geological Society, London, Special Publications, **135**, 307–326.

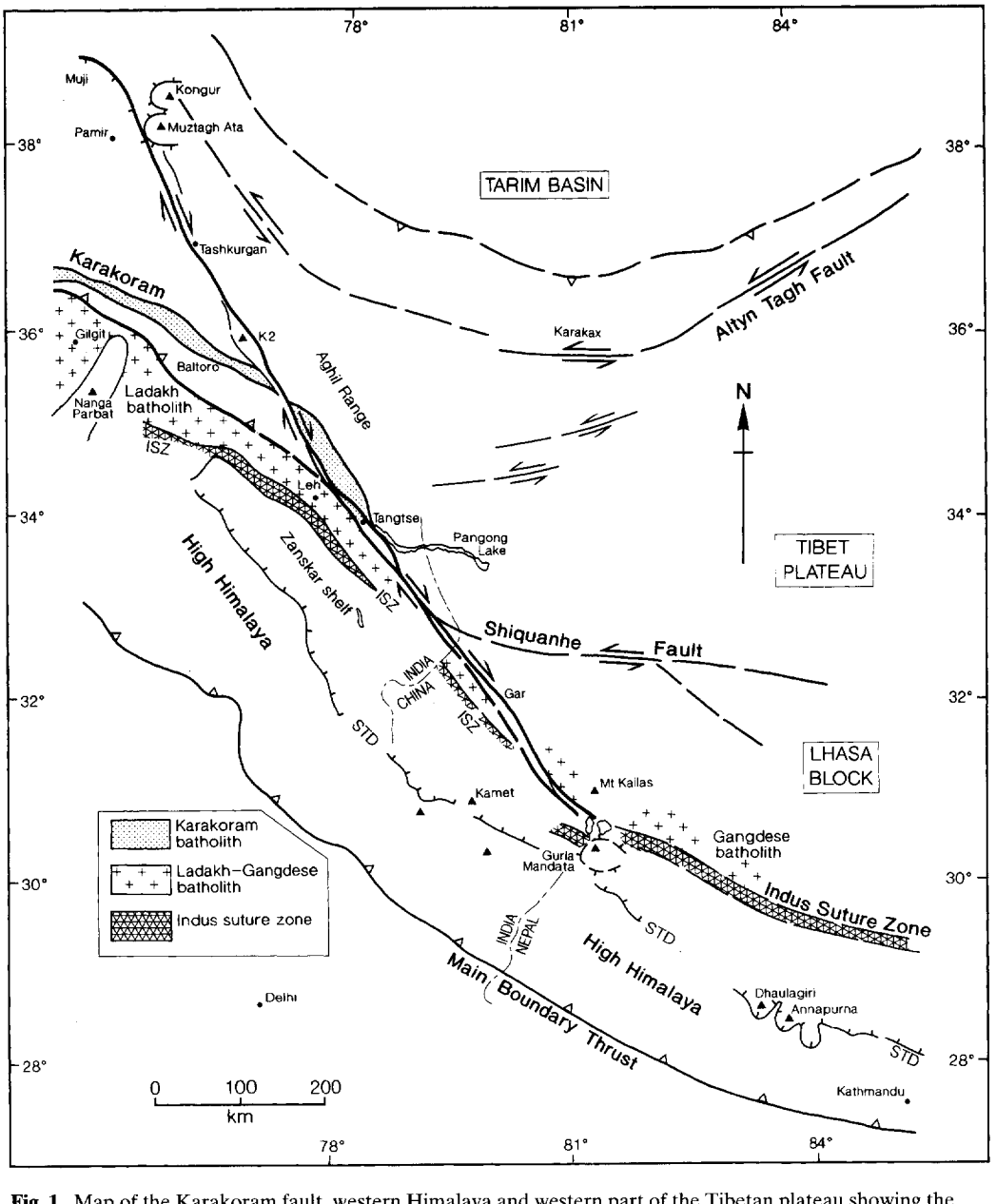

Fig. 1. Map of the Karakoram fault, western Himalaya and western part of the Tibetan plateau showing the major structures. ISZ, Indus suture zone; STD, South Tibetan Detachment system of normal faults which bounds the upper part of the High Himalayan slab.

(1993) and Liu *et al.* (1992) based on offset geomorphological features. However, as noted by Searle (1996), none of these Holocene slip rates are constrained by absolute ages on the displaced morphological features; all are assumed to have formed at the end of the last glaciation and the beginning of the Holocene warming period, which happened around 12 ± 2 ka, and, as pointed out by Gillespie & Molnar (1995), this age could be older by a factor of two to four.

Searle (1996) challenged the notion of *c.* 1000 km offset along the Karakoram fault by matching geological markers on either side of the fault. Using the well-dated Baltoro granites

(U–Pb zircon ages of 21 ± 0.5 Ma (Parrish & Tirrul 1989) and U–Pb monazite ages of 25.5 ± 0.3/−0.8 Ma (Schärer *et al.* 1990)) he demonstrated that *c.* 120 km of dextral offset had occurred since the early to mid-Miocene from the Bilafond glacier region of north Pakistan to the Shyok region of northern Ladakh (Fig. 2). Similar offsets of the Ladakh batholith, Shyok–Pangong suture and the offset course of the Indus river suggest that the fault initiated after formation of all of these geological features. By determining the age of the youngest of these features we can determine the maximum age of initiation of the fault.

In this paper we briefly review the zones of transpression and transtension along the Karakoram fault before discussing the geology of the northern Ladakh segment of the fault, where deep crustal metamorphic, migmatitic and leucogranitic rocks have been exhumed by transpression. We present new U–Pb SHRIMP and $^{40}Ar/^{39}Ar$ geochronological data, which are used to constrain dextral slip rates along the fault, and we discuss the evolution of the Karakoram fault, especially with regard to the major debate concerning the amount and timing of eastward extrusion of Tibetan crust.

Transpression and transtension along the Karakoram fault

The Karakoram fault stretches for some 1000 km from the Pamir mountains in the northwest to the Mt Kailas region in SW Tibet in the southeast (Fig. 1). Both ends of the fault terminate in a series of splays where transtensional basins are bounded by active normal faults. The northwestern termination of the fault in the central Pamirs shows active normal faults bounding the Muji graben around the Kongur and Muztagh Ata gneiss domes (Brunel *et al.* 1994; Searle 1996). The Tashkurgan graben south of Muztagh Ata is a transtensional pull-apart basin with the bounding faults showing both dextral strike-slip and dip-slip fabrics. The southeastern termination of the Karakoram fault in SW Tibet similarly shows a large-scale dextral transtensional pull-apart basin, the Gar basin, bounded by faults which show both strike-slip and dip-slip components (Armijo *et al.* 1989). Southeast of Gar, the Karakoram fault merges into the Indus suture zone in the region of Mt Kailas, where east–west normal faults parallel to the strike of the suture zone predominate.

The main dextral strike-slip motion occurs along the central segment of the fault, where several transpressionally uplifted mountain ranges are bounded by late Neogene or Quaternary faults which have both strike-slip and thrust-related kinematics associated with them. Examples are the K2–Gasherbrum range in northern Pakistan (Fig. 1) and the Pangong range in northern Ladakh, India (Figs 2 and 3).

K2 – Gasherbrum range

North of the Karakoram batholith in Pakistan and along the border of Ladakh (India) with western Tibet, a well-bedded sequence of Carboniferous black slates and Permian–Triassic massive carbonates form the Gasherbrum range (Fig. 2). These sediments have been intruded by Jurassic to early Cretaceous quartz diorites. Structural culminations of mid-crustal amphibolite-facies rocks, the K2 gneiss, have Cretaceous crystallization ages (U–Pb zircon ages 115–120 Ma), and K–Ar cooling ages of 111–94 Ma (Searle *et al.* 1990). The K2–Gasherbrum range forms a very high (8000–8600 m) barrier of mountains parallel to, and immediately SW of the Karakoram fault, which runs along the Shaksgam valley. North of K2, mylonites exposed along the fault in the Shaksgam valley separate amphibolite-facies rocks of the K2 gneiss to the southwest from unmetamorphosed carbonates of the Aghil range to the northeast (Searle 1991). Fission-track zircon ages from samples collected over the altitude range 4900–7150 m on Gasherbrum IV have a range from 125 to 31 Ma (Cerveny *et al.* 1989), indicating that only about 6 km of material has been eroded since the Cretaceous. Because of the very high present-day relief and deep erosion, most of this erosion must have occurred in very recent times. Fission-track apatite ages from K2 support this assumption, with samples collected over the altitude range 5300 – 8611 m giving ages of 4.3 ± 1.4 to 2.1 ± 0.6 Ma (Foster *et al.* 1994). Combined with the U–Pb zircon and K–Ar hornblende, muscovite and biotite ages (Searle *et al.* 1989, 1990), the cooling history of the K2 gneiss shows long slow cooling from 110 to *c.* 5 Ma and then extremely rapid erosion of about 6–7 km of material in the last 5 Ma. The deep crustal metamorphic rocks of K2 are bounded by faults on either side, which show both dextral strike-slip and normal fault kinematic indicators (Searle 1991). The higher exhumation rates, greater erosion and high present-day topography in the K2 range support the contention that it was uplifted by transpression during dextral shear along the Karakoram fault in the period from 5 to 0 Ma.

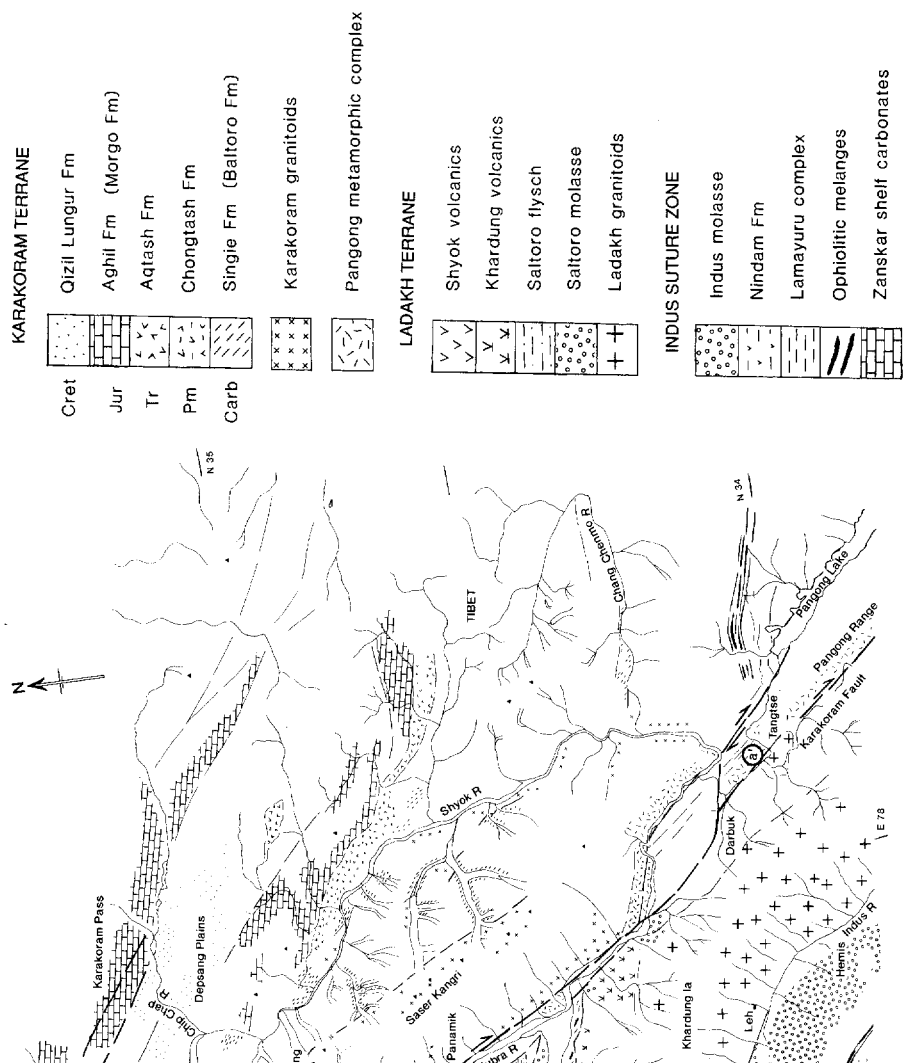

Fig. 2. Geological map of the central part of the Karakoram fault in the eastern Karakoram, modified after Searle (1996). 'a' (southern part of the Baltoro-type granites in the Saltoro Kangri–K12 region of northern Pakistan) and 'a'' (Darbuk–Tangtse area in northern Ladakh) mark the points offset dextrally along the Karakoram fault.

Fig. 3. Geological map o
approximately double thi
eastward bounded by the
north.

Pangong range

In the Shyok region of
ing bend is present wh
splays into two branc
northeastern Pangong
fault runs along the Sh
to the north end of the
the southern part of Pa
across the margin of

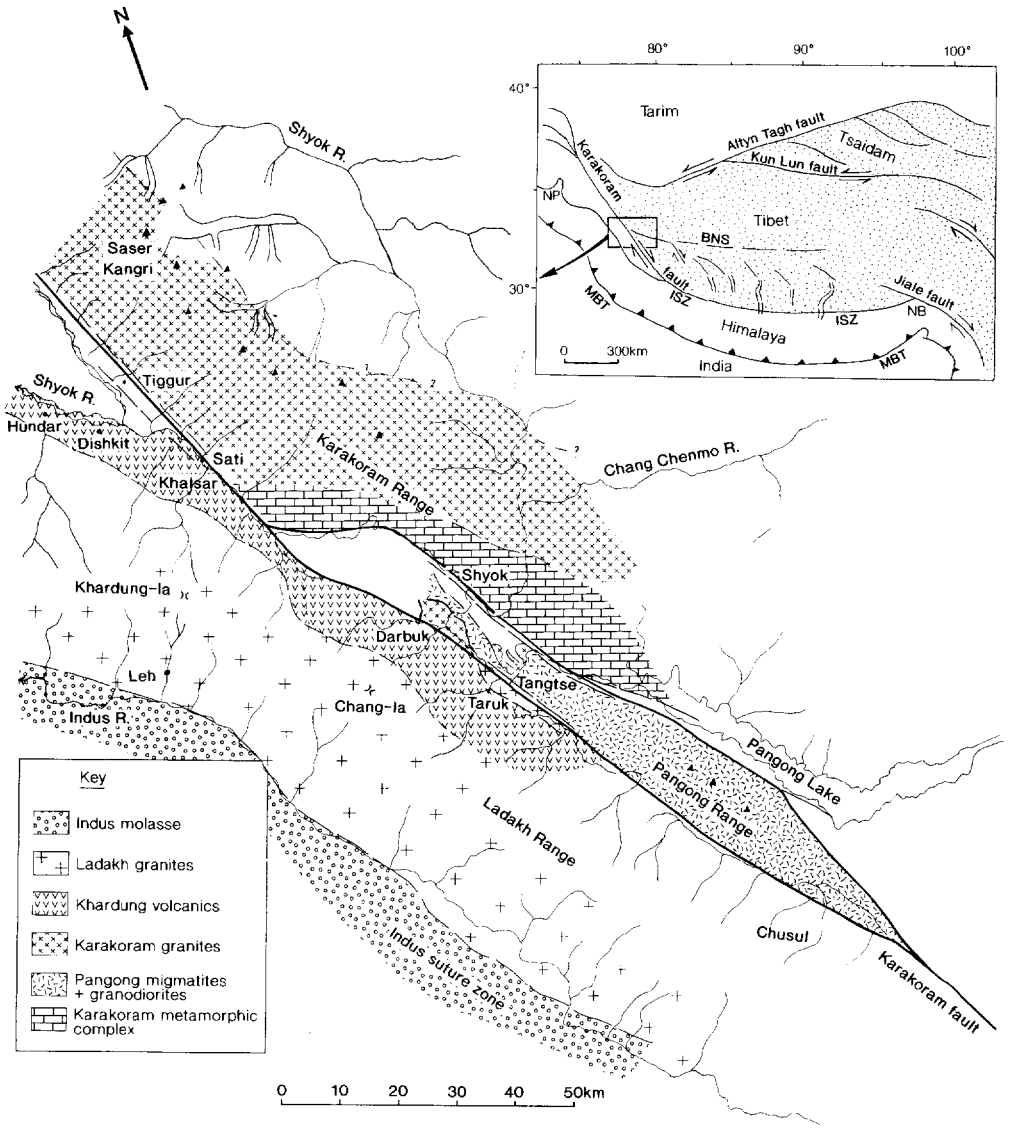

Fig. 2. Geological map of the central part of the Karakoram fault in the eastern Karakoram, modified after Searle (1996). 'a' (southern part of the Baltoro-type granites in the Saltoro Kangri–K12 region of northern Pakistan) and 'a'' (Darbuk–Tangtse area in northern Ladakh) mark the points offset dextrally along the Karakoram fault.

Fig. 3. Geological map of the Karakoram fault in northern Ladakh, India. Inset shows the area of approximately double thickness continental crust (shaded area), which, in the extrusion model, is moving eastward bounded by the dextral Karakoram fault in the southwest and the sinistral Altyn Tagh fault along the north.

Pangong range

In the Shyok region of Ladakh, a major restraining bend is present where the Karakoram fault splays into two branches (Figs 3 and 4). The northeastern Pangong strand of the Karakoram fault runs along the Shyok valley, and cuts across to the north end of the Tangtse gorge (Fig. 5) to the southern part of Pangong lake, where it cuts across the margin of the Pangong range. The Pangong lake is a drowned river valley which appears to have been dammed by recent movement along this branch of the Karakoram fault (Fig. 6). The southwestern branch, the Tangtse strand, runs through Darbuk and Tangtse villages towards Chusul and is the major fault which separates Karakoram terrane rocks to the northeast from pre-collisional Ladakh granites and Khardung volcanic rocks to the southwest. Southeast of Chusul both branches of the

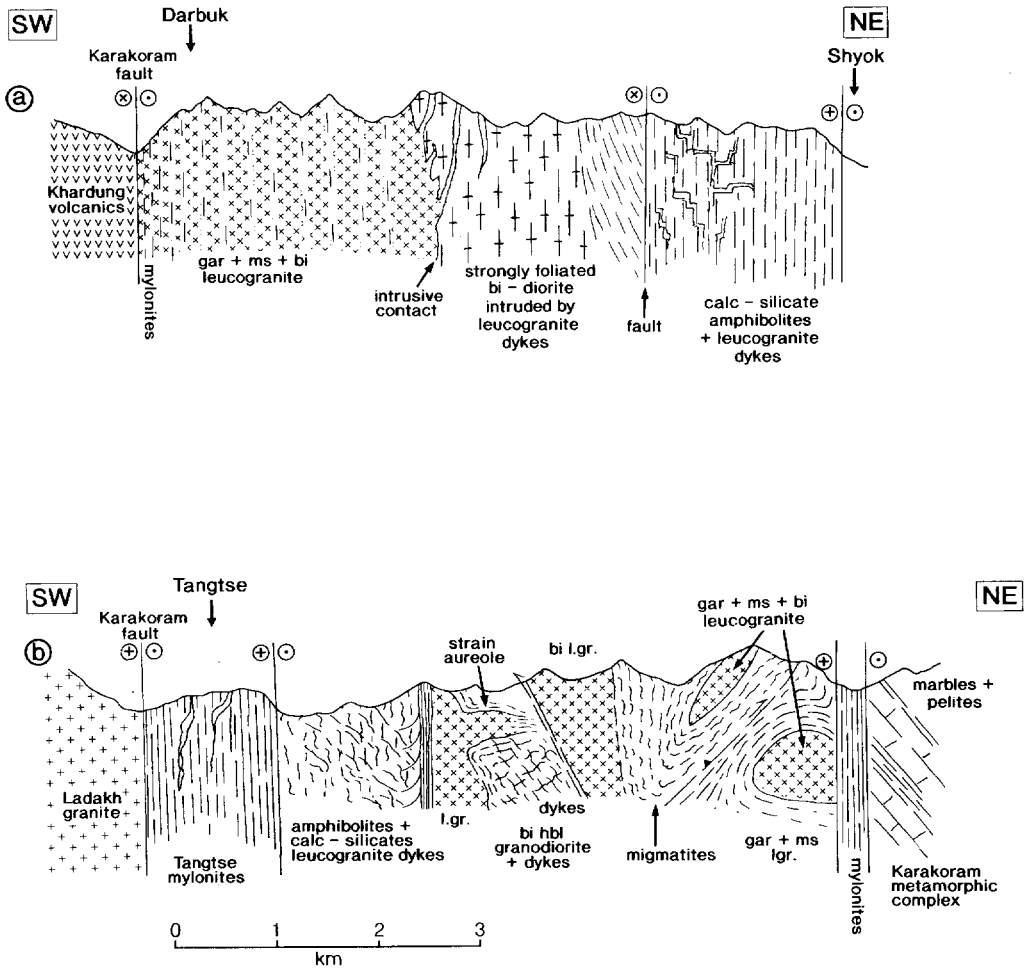

Fig. 4. Simplified cross-sections across the two strands of the Karakoram fault at Darbuk and Tangtse (see Fig. 3 for location).

Karakoram fault merge to form one dominant strand (Fig. 3).

The Pangong range is a transpressionally uplifted mountain belt rising to over 6500 m between these two strands of the Karakoram fault. Relative exhumation is shown by the high metamorphic grade of rocks within the range compared with lower-grade (greenschist-facies) volcano-sedimentary rocks to the northeast and virtually unmetamorphosed volcanic rocks of the Khardung Formation to the southwest. Preferential uplift of the Pangong range is also indicated by its greater surface topography compared with the flatter region northeast of the Pangong strand. Recent uplift of the Pangong range is synchronous with motion along the Pangong strand of the Karakoram fault. Hanging glaciers draining northeastwards off the Pangong range, south of Pangong lake, have been truncated by the fault, which also shows down-to-the-northeast movement.

Between the two strands, a variety of migmatites and high-grade metamorphic rocks including amphibolites, orthogneisses, calc-silicates and rare pelites are exposed. Amphibolites and granodioritic gneisses in the Pangong range containing biotite and hornblende show *in situ* partial melt textures forming migmatites. These rocks have been intruded by a network of quartzo-feldspathic pegmatites as well as biotite + muscovite ± garnet ± tourmaline leucogranite dykes and sheets (the Tangtse injection complex; Fig. 7), which locally come together to form kilometre-sized plutons (Weinberg & Searle in press).

Staurolite + garnet metapelitic schists occur

Fig. 5. Kilometre-sized plut
Karakoram fault, north of T
pluton after emplacement.

along the road leading to
deformed, more massive
ates and pelites occur no
strand of the Karakora
Karakoram metamorph
south of the batholith in
northern Ladakh the me
been inter-sheared wi
granites and Pangong
Karakoram fault zone.
deformation fabrics and
zone 800–1200 m wide a
the Karakoram fault (F
fabrics have been superi
undeformed Ladakh gr
Tangtse a strong myloni
tous, plunging at 20° tow
consistent with the obs
crustal rocks have beer
Karakoram fault in this a

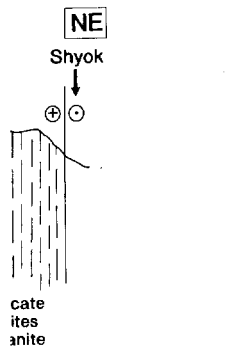

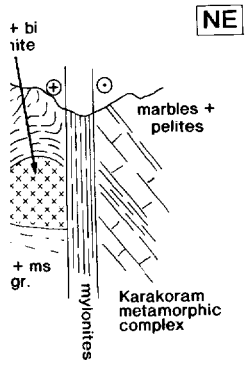

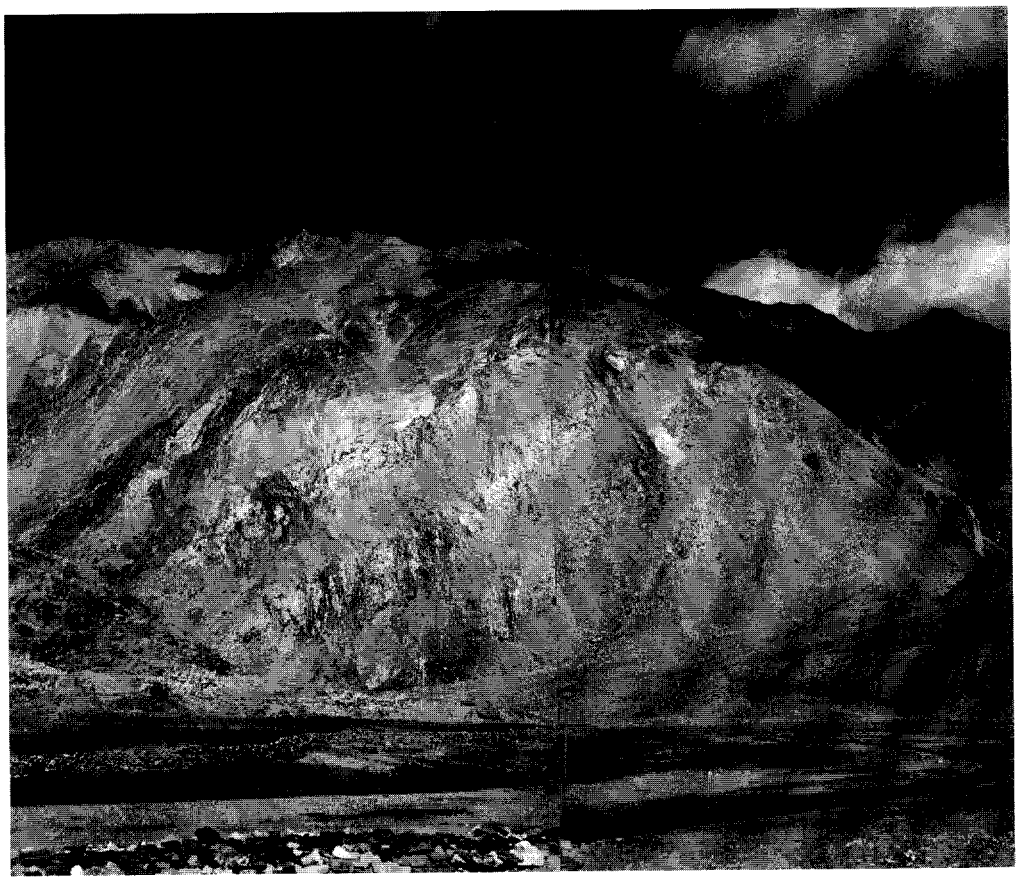

Fig. 5. Kilometre-sized pluton of a two-mica + garnet leucogranite adjacent to the northeastern strand of the Karakoram fault, north of Tangtse. Foliation in the surroundings was deformed into concordance with the pluton after emplacement.

rbuk and Tangtse (see Fig.

of Pangong lake, have
fault, which also shows
novement.
strands, a variety of
ade metamorphic rocks
orthogneisses, calc-sili-
e exposed. Amphibolites
es in the Pangong range
hornblende show *in situ*
ming migmatites. These
ded by a network of
matites as well as biotite
tourmaline leucogranite
the Tangtse injection
locally come together to
plutons (Weinberg &

netapelitic schists occur

along the road leading to Pangong lake, and less deformed, more massive bedded meta-carbonates and pelites occur northeast of the Pangong strand of the Karakoram fault. Whereas the Karakoram metamorphic complex crops out south of the batholith in the Pakistan sector, in northern Ladakh the metamorphic rocks have been inter-sheared with the Baltoro-type granites and Pangong migmatites along the Karakoram fault zone. All rocks show strong deformation fabrics and mylonites outcrop in a zone 800–1200 m wide along both branches of the Karakoram fault (Fig. 4). Dextral shear fabrics have been superimposed on previously undeformed Ladakh granite lithologies. At Tangtse a strong mylonitic lineation is ubiquitous, plunging at 20° towards the NW. This is consistent with the observation that deeper crustal rocks have been exhumed along the Karakoram fault in this area.

SHRIMP U–Pb zircon dating from the migmatites reveals core ages of 106.3 ± 2.3 Ma (see below). Based on the lithogical and age similarities, the Pangong migmatites are correlated with similar, pre-collisional, deformed granodioritic rocks in northern Pakistan, notably the K2 gneiss (Searle *et al.* 1990), the Muztagh Tower gneiss and the Hushe gneiss, which are also intruded by garnet leucogranite dykes (Searle 1991; Crawford & Searle 1992).

Offset Karakoram granites

One of the youngest features displaced by the Karakoram fault is the Karakoram batholith. The youngest phase of granite magmatism within the Karakoram batholith is the middle Miocene Baltoro plutonic unit. Searle (1996) originally proposed 120 km of dextral offset of the Baltoro-type granites along the Karakoram

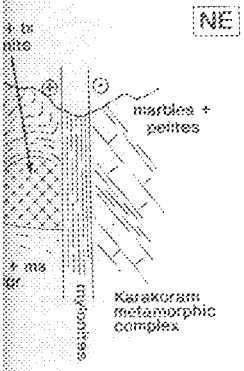

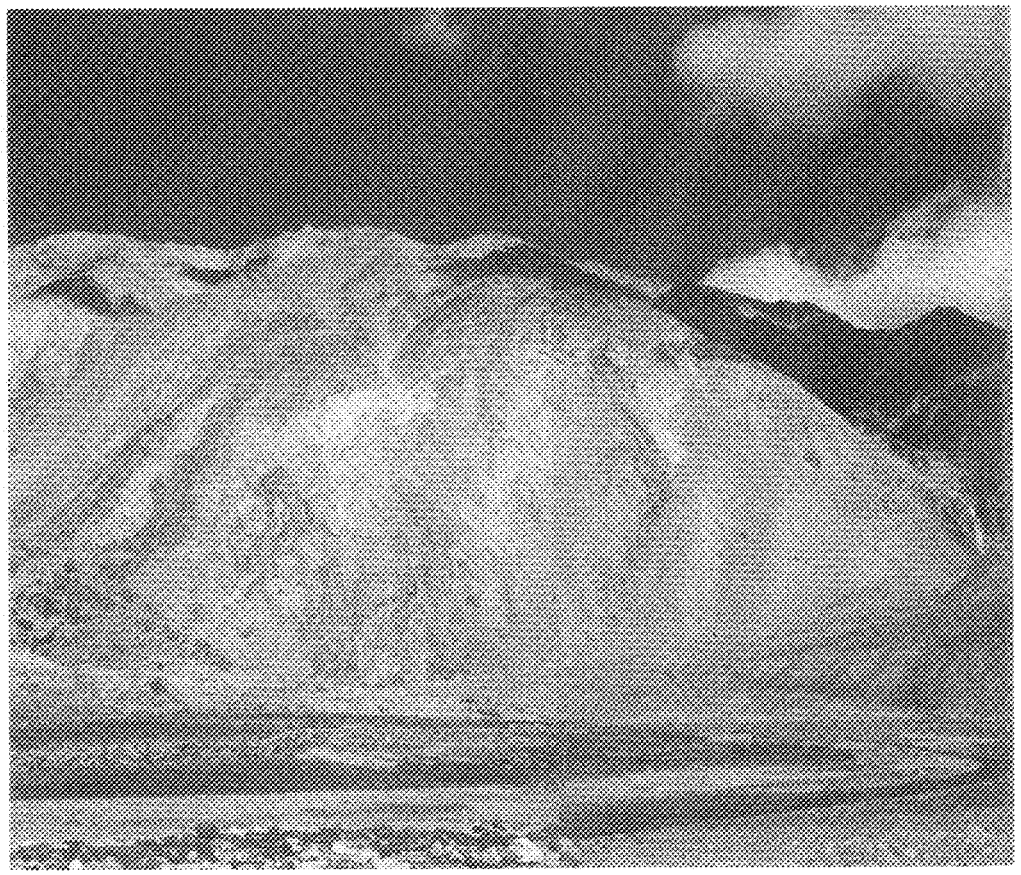

Fig. 5. Kilometre-sized pluton of a two-mica + garnet leucogranite adjacent to the northeastern strand of the Karakoram fault, north of Tangtse. Foliation in the surroundings was deformed into concordance with the pluton after emplacement.

rbuk and Tangtse (see Fig.

of Pangong lake, have fault, which also shows movement.

strands, a variety of ade metamorphic rocks orthogneisses, calc-silic- exposed. Amphibolites es in the Pangong range hornblende show *in situ* ming migmatites. These ded by a network of mantles as well as biotite tourmaline leucogranite the Tangtse injection locally come together to plutons (Weinberg &

metapelitic schists occur along the road leading to Pangong lake, and less deformed, more massive bedded meta-carbonates and pelites occur northeast of the Pangong strand of the Karakoram fault. Whereas the Karakoram metamorphic complex crops out south of the batholith in the Pakistan sector, in northern Ladakh the metamorphic rocks have been inter-sheared with the Baltoro-type granites and Pangong migmatites along the Karakoram fault zone. All rocks show strong deformation fabrics and mylonites outcrop in a zone 800–1200 m wide along both branches of the Karakoram fault (Fig. 4). Dextral shear fabrics have been superimposed on previously undeformed Ladakh granite lithologies. At Tangtse a strong mylonitic lineation is ubiquitous, plunging at 20° towards the NW. This is consistent with the observation that deeper crustal rocks have been exhumed along the Karakoram fault in this area.

SHRIMP U–Pb zircon dating from the migmatites reveals core ages of 106.3 ± 2.3 Ma (see below). Based on the lithogical and age similarities, the Pangong migmatites are correlated with similar, pre-collisional, deformed granodioritic rocks in northern Pakistan, notably the K2 gneiss (Searle *et al.* 1990), the Muztagh Tower gneiss and the Hushe gneiss, which are also intruded by garnet leucogranite dykes (Searle 1991; Crawford & Searle 1992).

Offset Karakoram granites

One of the youngest features displaced by the Karakoram fault is the Karakoram batholith. The youngest phase of granite magmatism within the Karakoram batholith is the middle Miocene Baltoro plutonic unit. Searle (1996) originally proposed 120 km of dextral offset of the Baltoro-type granites along the Karakoram

Fig. 6. The northeastern strand of the Karakoram fault runs along the Pangong Lake, which is a drowned river valley, dammed by transpressional uplift at its western end.

Fig. 7. Two-mica leucogr
Injection Complex) intru
silicates and pelites within
north of Tangtse village.

fault. Following our more detailed regional mapping in north Ladakh, we now refine this value to 150 km based on the offset points shown in Fig. 2.

Baltoro granite

The Baltoro granite forms a large component of the Karakoram batholith in northern Pakistan, where it consists of co-magmatic monzogranites and leucogranites with the assemblage qtz + Kfs+ pl + bt ± ms ± grt (Searle *et al.* 1989, 1992; Searle 1991). The Baltoro granites are mildly peraluminous with $^{87}Sr/^{86}Sr$ ratios of 0.7072–0.7128, and have geochemical characteristics compatible with dehydration melting of a biotite-rich pelite in a lower-crustal source (Rex *et al.* 1988). The Baltoro granite intrudes sillimanite grade gneisses along the southern margin and unmetamorphosed Carboniferous–Permian and Mesozoic sediments along the northern boundary, which have been contact metamorphosed along the margin to form andalusite hornfels (Searle *et al.* 1989, 1992). The age of crustal melting is known from U–Pb zircon ages of 21.0 ± 0.5 Ma from samples collected along the Baltoro glacier (Parrish & Tirrul 1989) and U–Pb monazite ages of $25.5^{+0.5}/_{-0.8}$ Ma from the Latok peaks, west of the Baltoro (Scharer *et al.* 1990). A suite of lamprophyre dykes (hornblende vogesites and biotite minettes) intrude the country rocks north of the Baltoro granite and a few occur south of the batholith in Hushe. Two of these lamprophyres from Broad Peak and the Abruzzi glacier have K–Ar biotite ages of 22.0 ± 0.7 Ma and 22.4 ± 0.7 Ma, and one from the Masherbrum glacier south of the batholith has a K–Ar biotite age of 24.0 ± 1.0 Ma (Searle *et al.* 1989). These volatile-rich, mantle-derived melts were therefore intruded at the same time as the lower-crustal melts forming the Baltoro granite. Because of the volume of lower-crustal melting along the central Karakoram, which is far greater than the volume of crustal melt granites along the High Himalaya, and the synchroneity of the lamprophyre dyke intrusion, Searle *et al.* (1992) proposed a model involving simultaneous lower-crustal and upper-mantle melting at *c.* 21 Ma beneath the Karakoram, with mantle melts providing an additional source of heat to promote widespread lower-crustal melting.

In the Baltoro and northern Hushe regions of north Pakistan, the Baltoro granites are undeformed with intrusive contacts along both north and south margins. These monzogranites and

leucogranites continue
Kangri–K12 range
extremely high and lar
right on the disputed b
Pakistan. The position
the location where the
type granites have bee
fault. South of this p
leucogranites of simila
tion to the Baltoro un
cuts the batholith at an
of the batholith has be
of the fault into paralle
Siachen glacier region
deformation in the form
has been superimposed
along the Karakoram
therefore have been a
of the granites at *c.* 25–

Tangtse granite

Larger leucogranite
Karakoram fault zone

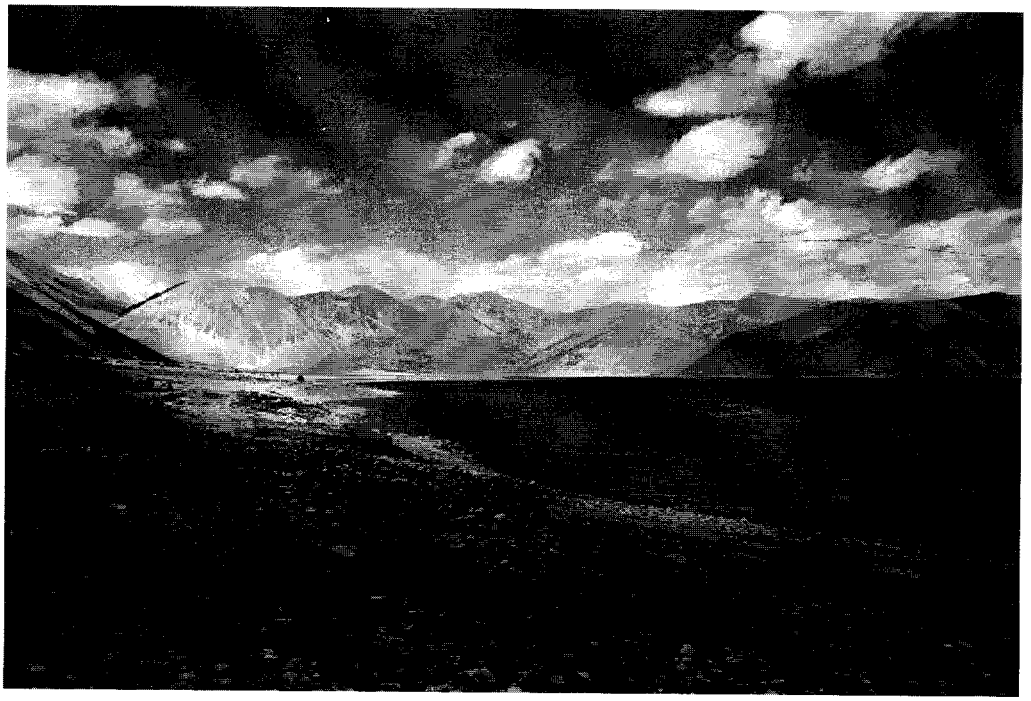

Fig. 6. The northeastern strand of the Karakoram fault runs along the Pangong Lake, which is a drowned river valley, dammed by transpressional uplift at its western end.

Fig. 7. Two-mica leucogr
Injection Complex) intru
silicates and pelites withi
north of Tangtse village.

fault. Following our more detailed regional mapping in north Ladakh, we now refine this value to 150 km based on the offset points shown in Fig. 2.

Baltoro granite

The Baltoro granite forms a large component of the Karakoram batholith in northern Pakistan, where it consists of co-magmatic monzogranites and leucogranites with the assemblage qtz + Kfs+ pl + bt ± ms ± grt (Searle *et al.* 1989, 1992; Searle 1991). The Baltoro granites are mildly peraluminous with $^{87}Sr/^{86}Sr$ ratios of 0.7072–0.7128, and have geochemical characteristics compatible with dehydration melting of a biotite-rich pelite in a lower-crustal source (Rex *et al.* 1988). The Baltoro granite intrudes sillimanite grade gneisses along the southern margin and unmetamorphosed Carboniferous–Permian and Mesozoic sediments along the northern boundary, which have been contact metamorphosed along the margin to form andalusite hornfels (Searle *et al.* 1989, 1992). The age of crustal melting is known from U–Pb zircon ages of 21.0 ± 0.5 Ma from samples collected along the Baltoro glacier (Parrish & Tirrul 1989) and U–Pb monazite ages of $25.5\ ^{+0.3}/_{-0.8}$ Ma from the Latok peaks, west of the Baltoro (Schärer *et al.* 1990). A suite of lamprophyre dykes (hornblende vogesites and biotite minettes) intrude the country rocks north of the Baltoro granite and a few occur south of the batholith in Hushe. Two of these lamprophyres from Broad Peak and the Abruzzi glacier have K–Ar biotite ages of 22.0 ± 0.7 Ma and 22.4 ± 0.7 Ma, and one from the Masherbrum glacier south of the batholith has a K–Ar biotite age of 24.0 ± 1.0 Ma (Searle *et al.* 1989). These volatile-rich, mantle-derived melts were therefore intruded at the same time as the lower-crustal melts forming the Baltoro granite. Because of the volume of lower-crustal melting along the central Karakoram, which is far greater than the volume of crustal melt granites along the High Himalaya, and the synchroneity of the lamprophyre dyke intrusion, Searle *et al.* (1992) proposed a model involving simultaneous lower-crustal and upper-mantle melting at *c.* 21 Ma beneath the Karakoram, with mantle melts providing an additional source of heat to promote widespread lower-crustal melting.

In the Baltoro and northern Hushe regions of north Pakistan, the Baltoro granites are undeformed with intrusive contacts along both north and south margins. These monzogranites and

leucogranites continue
Kangri–K12 range
extremely high and lar
right on the disputed b
Pakistan. The position
the location where the
type granites have bee
fault. South of this p
leucogranites of simila
tion to the Baltoro un
cuts the batholith at an
of the batholith has be
of the fault into paralle
Siachen glacier region
deformation in the form
has been superimposed
along the Karakoram
therefore have been a
of the granites at *c.* 25–

Tangtse granite

Larger leucogranite
Karakoram fault zone

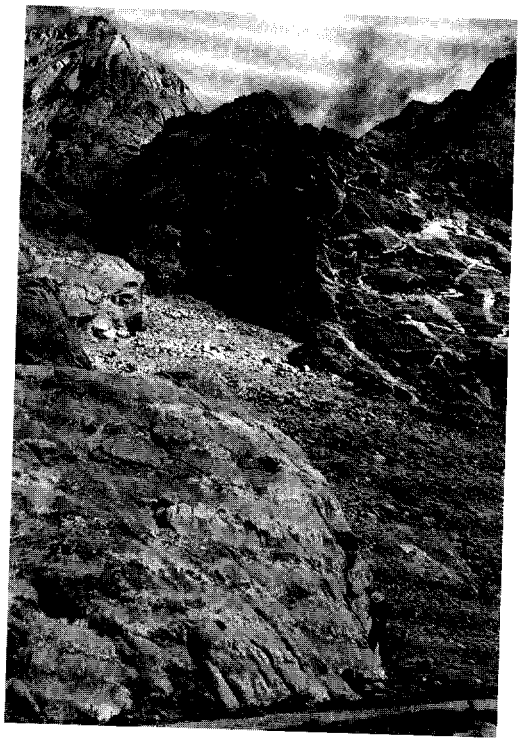

Fig. 7. Two-mica leucogranite dykes (Pangong Injection Complex) intruding amphibolites, calc-silicates and pelites within the Karakoram fault zone, north of Tangtse village.

leucogranites continue eastward to the Saltoro Kangri–K12 range (Fig. 2). This area is extremely high and largely inaccessible, and lies right on the disputed border between India and Pakistan. The position marked 'a' in Fig. 2 marks the location where the upper Miocene Baltoro-type granites have been cut by the Karakoram fault. South of this point there are no more leucogranites of similar mineralogy or composition to the Baltoro unit. The Karakoram fault cuts the batholith at an acute angle and the trend of the batholith has been rotated clockwise NE of the fault into parallel alignment with it in the Siachen glacier region (Searle 1996). Solid-state deformation in the form of mylonitic S–C fabrics has been superimposed on the Baltoro granites along the Karakoram fault. The fault must therefore have been active after crystallization of the granites at *c.* 25–21 Ma.

Tangtse granite

Larger leucogranite intrusions within the Karakoram fault zone at Darbuk and Tangtse (Figs 3 and 4) contain biotite, muscovite and garnet, and were also intruded before movement along the Karakoram fault. Spectacular dextral S–C fabrics (Fig. 8) have been superimposed on the igneous texture. These leucogranites are compositionally similar to the Baltoro leucogranite in Pakistan and we correlate the two as originally belonging to the same batholith. Their similar mineralogy, trace element contents, and Rb/Sr and Rb/Ba ratios (normalized to primordial mantle values from Taylor & McLennan (1985)) strongly contrast with those of the neighbouring Ladakh granite. Furthermore, as we will show below, the ages of the Baltoro and the Tangtse granites are both early to mid-Miocene, and contrast with the much older, pre-collisional Ladakh granites (which span the range 103–50 Ma). The leucogranites have been offset dextrally along the Karakoram fault for a maximum of 150 km from the Saltoro Kangri–K12 range southwest of the Karakoram fault in Pakistan to the Darbuk–Tangtse area in north Ladakh (Fig. 2). The fact that no Baltoro–Tangtse-type granites occur southwest of the Karakoram fault in Ladakh strongly suggests that the Karakoram fault initiated after 18.0 ± 0.6 Ma (2σ), the crystallization age of the youngest offset granite (see below).

The Tangtse granite intruded earlier, foliated, biotite-rich diorite, migmatites, calc-silicates and pelites, and has been intensely deformed by non-coaxial dextral shear in the greenschist facies along the Karakoram fault after crystallization. Solid-state deformation is defined by strong S–C fabrics indicative of dextral shear. Although the entire granite is deformed, the S–C fabrics are best developed along the southwestern margin of the Karakoram fault zone. Microstructures suggest that deformation of the Tangtse leucogranite occurred under greenschist facies conditions (450–300°C) and there is no evidence of a high-temperature deformation history. The quartz exhibits ductile deformation features only, with the grains having accommodated strain by both grain boundary migration recrystallization and sub-grain rotation. The K-feldspar in the leucogranite has deformed mainly by fracturing and cataclastic flow, which is characteristic of granites deformed under greenschist-facies conditions.

U–Pb and $^{40}Ar/^{39}Ar$ geochronology was undertaken on key samples of Tangtse granite and rocks on either side of the Karakoram fault, to determine the age of strike-slip faulting and the cooling history of rocks within the Karakoram fault and to the southwest in the Ladakh batholith.

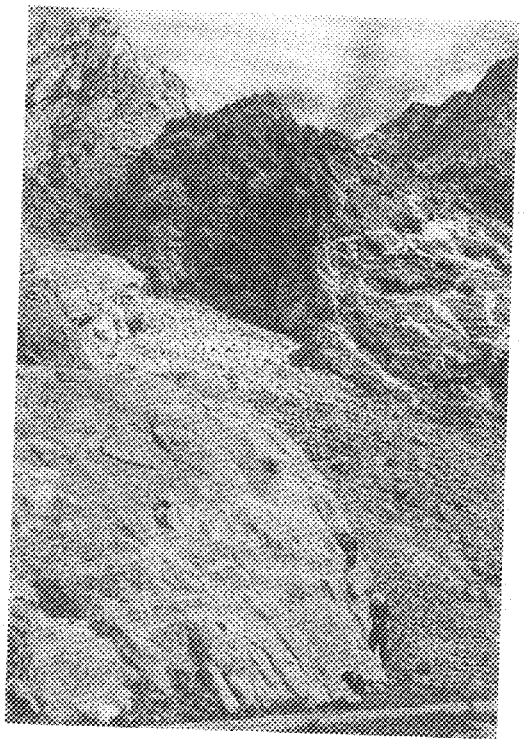

Fig. 7. Two-mica leucogranite dykes (Pangong Injection Complex) intruding amphibolites, calc-silicates and pelites within the Karakoram fault zone, north of Tangtse village.

leucogranites continue eastward to the Saltoro Kangri–K12 range (Fig. 2). This area is extremely high and largely inaccessible, and lies right on the disputed border between India and Pakistan. The position marked 'a' in Fig. 2 marks the location where the upper Miocene Baltoro-type granites have been cut by the Karakoram fault. South of this point there are no more leucogranites of similar mineralogy or composition to the Baltoro unit. The Karakoram fault cuts the batholith at an acute angle and the trend of the batholith has been rotated clockwise NE of the fault into parallel alignment with it in the Siachen glacier region (Searle 1996). Solid-state deformation in the form of mylonitic S–C fabrics has been superimposed on the Baltoro granites along the Karakoram fault. The fault must therefore have been active after crystallization of the granites at *c.* 25–21 Ma.

Tangtse granite

Larger leucogranite intrusions within the Karakoram fault zone at Darbuk and Tangtse (Figs 3 and 4) contain biotite, muscovite and garnet, and were also intruded before movement along the Karakoram fault. Spectacular dextral S–C fabrics (Fig. 8) have been superimposed on the igneous texture. These leucogranites are compositionally similar to the Baltoro leucogranite in Pakistan and we correlate the two as originally belonging to the same batholith. Their similar mineralogy, trace element contents, and Rb/Sr and Rb/Ba ratios (normalized to primordial mantle values from Taylor & McLennan (1985)) strongly contrast with those of the neighbouring Ladakh granite. Furthermore, as we will show below, the ages of the Baltoro and the Tangtse granites are both early to mid-Miocene, and contrast with the much older, pre-collisional Ladakh granites (which span the range 103–50 Ma). The leucogranites have been offset dextrally along the Karakoram fault for a maximum of 150 km from the Saltoro Kangri–K12 range southwest of the Karakoram fault in Pakistan to the Darbuk–Tangtse area in north Ladakh (Fig. 2). The fact that no Baltoro–Tangtse-type granites occur southwest of the Karakoram fault in Ladakh strongly suggests that the Karakoram fault initiated after 18.0 ± 0.6 Ma (2σ), the crystallization age of the youngest offset granite (see below).

The Tangtse granite intruded earlier, foliated, biotite-rich diorite, migmatites, calc-silicates and pelites, and has been intensely deformed by non-coaxial dextral shear in the greenschist facies along the Karakoram fault after crystallization. Solid-state deformation is defined by strong S–C fabrics indicative of dextral shear. Although the entire granite is deformed, the S–C fabrics are best developed along the southwestern margin of the Karakoram fault zone. Microstructures suggest that deformation of the Tangtse leucogranite occurred under greenschist facies conditions (450–300°C) and there is no evidence of a high-temperature deformation history. The quartz exhibits ductile deformation features only, with the grains having accommodated strain by both grain boundary migration recrystallization and sub-grain rotation. The K-feldspar in the leucogranite has deformed mainly by fracturing and cataclastic flow, which is characteristic of granites deformed under greenschist-facies conditions.

U–Pb and $^{40}Ar/^{39}Ar$ geochronology was undertaken on key samples of Tangtse granite and rocks on either side of the Karakoram fault, to determine the age of strike-slip faulting and the cooling history of rocks within the Karakoram fault and to the southwest in the Ladakh batholith.

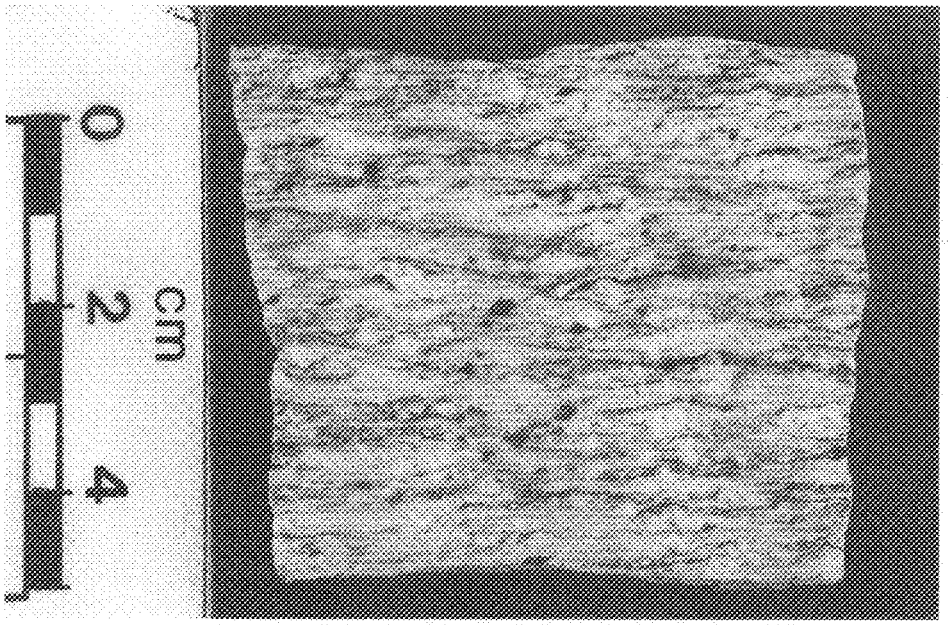

Fig. 8. Polished slab of Tangtse granite from the southwestern strand of the Karakoram fault near Tangtse village, showing spectacular dextral S–C fabrics.

U–Pb SHRIMP dating

Two samples were prepared for U–Pb dating using the Sensitive High-Resolution Microprobe (SHRIMP II) at the Australian National University. A sample of the granite from the *in situ* Pangong migmatite was collected in the Tangtse gorge (sample 022), and a sample of the mylonitic Tangtse leucogranite was collected between the villages of Tangtse and Darbuk (sample 215). The leucogranite sample is particularly important because its crystallization age provides a maximum age for the initiation of the dextral shear along the Karakoram fault.

The Tangtse granite, sample 215, has prismatic, 150–400 μm long zircons. Cathodoluminescence (CL) images show that these zircons generally have luminescent (low U) cores with euhedral fine-scale oscillatory igneous zoning, truncated and overgrown by weakly luminescent (high U) finely zoned prismatic mantles. Primary ion beams were focused to spots of *c.* 30 μm in diameter, and using the CL images we dated the cores and mantles and avoided overlapping the two distinct domains (overlap occurred, however, in spot 9.2 (Table 1) as found in CL images produced after analysis; this spot was not included in the plots of Fig. 9). Details of the procedure for zircon U–Pb isotopic analysis using the SHRIMP have been given by Compston *et al.* (1984) and Williams & Claesson (1987), and the standard used was SL13 (Claoué-Long *et al.* 1995). During analysis, for every four spots of unknown sample, two standards were analysed. For each analysis, seven cycles of secondary ion yields were measured on the following ions: Zr_2O^+, the four lead isotopes (^{208}Pb, ^{207}Pb, ^{206}Pb, ^{204}Pb), U^+ and UO^+, Th^+ and ThO^+. Because neither $^{207}Pb/^{206}Pb$ nor $^{207}Pb/^{235}U$ chronology by SHRIMP provides a fine age resolution for the Phanerozoic, we relied entirely on the $^{206}Pb/^{238}U$ and when possible on $^{208}Pb/^{232}Th$ geochronometers. The procedure to determine the errors associated with the unknown ages has been described by Claoué-Long *et al.* (1992), and includes the error of the UO/U v. $^{206}Pb/^{238}U$ calibration line, and the counting statistics error of the unknowns. The capability of the SHRIMP in resolving the age of young rocks has been shown by Zeitler *et al.* (1989), who successfully dated thin zircon rims younger than 11 Ma. In total we analysed 39 spots in 23 zircons (Table 1). We corrected the results for common lead by assuming the isotopic composition of lead from Broken Hill, Australia.

The results may be divided into two age groups and a few scattered values (Fig. 9a, Table 1). The older group represents inherited zircons from the magma source and the younger group

T

Table 1. *SHRIMP analyse*

Spot	Date	Core (1) or rim (2)	U (pp
1.1	23.06	1	484
1.2	23.09	2	1578
2.1	23.06	2	145
2.2	23.06	1	1056
3.1	23.06	1	182
4.1	23.06	1	45
4.2	23.06	2	1131
5.1	23.06	2	396
5.2	23.06	1	406
6.1	23.06	1	35
7.1	23.06	1	65
7.2	23.06	2	1362
8.1	23.06	1	10
8.2	23.06	2	609
9.1	23.06	1	38
9.2	23.06	2	56
10.1	23.06	1	110
10.2	23.09	2	748
11.1	23.06	1	6
11.2	23.06	2	707
11.3	23.06	1	8
12.1	23.06	1	94
12.2	23.06	2	1413
13.1	23.06	1	93
14.1	23.06	1	67
14.2	23.09	2	1348
15.1	23.06	1	138
16.1	23.06	1	32
16.2	23.06	2	795
17.1	23.06	1	351
18.1	23.06	1	84
19.1	23.06	1	136
19.2	23.06	2	517
20.1	23.06	1	130
20.2	23.06	0	72
20.3	23.09	2	922
21.1	23.09	2	1220
22.1	23.09	2	1598
22.2	23.09	1	39
23.1	23.09	2	1364

%206c indicates the perce
percentage of commo
correspond to poorly

represents the age o
Tangtse granite. Six dat
group with a weighted
(2σ) and four data po
decreasing from *c.* 60 to
grains were affected by
same zircon yielded m
and 920 Ma (Table 1), s
older crustal rocks. On
(Table 1, Fig. 9a), wh

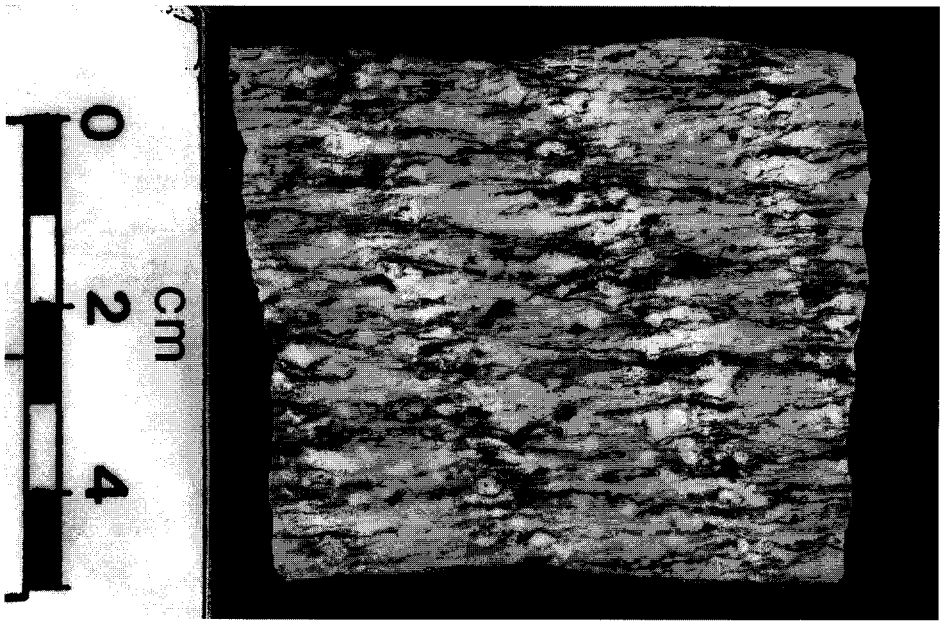

Fig. 8. Polished slab of Tangtse granite from the southwestern strand of the Karakoram fault near Tangtse village, showing spectacular dextral S–C fabrics.

U–Pb SHRIMP dating

Two samples were prepared for U–Pb dating using the Sensitive High-Resolution Microprobe (SHRIMP II) at the Australian National University. A sample of the granite from the *in situ* Pangong migmatite was collected in the Tangtse gorge (sample 022), and a sample of the mylonitic Tangtse leucogranite was collected between the villages of Tangtse and Darbuk (sample 215). The leucogranite sample is particularly important because its crystallization age provides a maximum age for the initiation of the dextral shear along the Karakoram fault.

The Tangtse granite, sample 215, has prismatic, 150–400 μm long zircons. Cathodoluminescence (CL) images show that these zircons generally have luminescent (low U) cores with euhedral fine-scale oscillatory igneous zoning, truncated and overgrown by weakly luminescent (high U) finely zoned prismatic mantles. Primary ion beams were focused to spots of *c.* 30 μm in diameter, and using the CL images we dated the cores and mantles and avoided overlapping the two distinct domains (overlap occurred, however, in spot 9.2 (Table 1) as found in CL images produced after analysis; this spot was not included in the plots of Fig. 9). Details of the procedure for zircon U–Pb isotopic analysis using the SHRIMP have been given by Compston *et al.* (1984) and Williams & Claesson (1987), and the standard used was SL13 (Claoué-Long *et al.* 1995). During analysis, for every four spots of unknown sample, two standards were analysed. For each analysis, seven cycles of secondary ion yields were measured on the following ions: Zr_2O^+, the four lead isotopes (^{208}Pb, ^{207}Pb, ^{206}Pb, ^{204}Pb), U^+ and UO^+, Th^+ and ThO^+. Because neither $^{207}Pb/^{206}Pb$ nor $^{207}Pb/^{235}U$ chronology by SHRIMP provides a fine age resolution for the Phanerozoic, we relied entirely on the $^{206}Pb/^{238}U$ and when possible on $^{208}Pb/^{232}Th$ geochronometers. The procedure to determine the errors associated with the unknown ages has been described by Claoué-Long *et al.* (1992), and includes the error of the UO/U v. $^{206}Pb/^{238}U$ calibration line, and the counting statistics error of the unknowns. The capability of the SHRIMP in resolving the age of young rocks has been shown by Zeitler *et al.* (1989), who successfully dated thin zircon rims younger than 11 Ma. In total we analysed 39 spots in 23 zircons (Table 1). We corrected the results for common lead by assuming the isotopic composition of lead from Broken Hill, Australia.

The results may be divided into two age groups and a few scattered values (Fig. 9a, Table 1). The older group represents inherited zircons from the magma source and the younger group

T

Table 1. *SHRIMP analyse*

Spot	Date	Core (1) or rim (2)	U (pp
1.1	23.06	1	484
1.2	23.09	2	1578
2.1	23.06	2	145
2.2	23.06	1	1056
3.1	23.06	1	182
4.1	23.06	1	44
4.2	23.06	2	1131
5.1	23.06	2	396
5.2	23.06	1	409
6.1	23.06	1	18
7.1	23.06	1	65
7.2	23.06	2	1362
8.1	23.06	1	10
8.2	23.06	2	609
9.1	23.06	1	38
9.2	23.06	2	56
10.1	23.06	1	110
10.2	23.09	2	748
11.1	23.06	1	6
11.2	23.06	2	707
11.3	23.06	1	8
12.1	23.06	1	94
12.2	23.06	2	1413
13.1	23.06	1	93
14.1	23.06	1	63
14.2	23.09	2	1348
15.1	23.06	1	138
16.1	23.06	1	32
16.2	23.06	2	795
17.1	23.06	1	351
18.1	23.06	1	84
19.1	23.06	1	136
19.2	23.06	2	517
20.1	23.06	1	130
20.2	23.06	0	72
20.3	23.09	2	922
21.1	23.09	2	1220
22.1	23.09	2	1598
22.2	23.09	1	39
23.1	23.09	2	1364

%206c indicates the perce
percentage of commo
correspond to poorly

represents the age o
Tangtse granite. Six dat
group with a weighted
(2σ) and four data po
decreasing from *c.* 60 to
grains were affected by
same zircon yielded mu
and 920 Ma (Table 1), su
older crustal rocks. On
(Table 1, Fig. 9a), wh

Table 1. *SHRIMP analyses of zircons from the Tangtse leucogranite sample 215*

Spot	Date	Core (1) or rim (2)	U (ppm)	Th (ppm)	%206c	%208c	$^{207}Pb/^{206}Pb$	$^{238}U/^{206}Pb$	$^{208}Pb/^{232}Th$ age (1σ)	$^{206}Pb/^{238}U$ age (1σ)
1.1	23.06	1	4845.0	1143	−0.01	−0.4	0.0463 ± 7	307.4 ± 2.7	18.7 ± 0.5	20.9 ± 0.2
1.2	23.09	2	15782.0	317	0.13	45.9	0.0477 ± 10	326.5 ± 4.6	9.3 ± 6.4	19.7 ± 0.3
2.1	23.06	2	1456.0	837	0.21	2.4	0.0483 ± 12	346.1 ± 3.4	18.2 ± 0.5	18.6 ± 0.2
2.2	23.06	1	10562.0	257	0.09	23.5	0.0473 ± 8	335.5 ± 5.9	13.2 ± 3.7	19.2 ± 0.3
3.1	23.06	1	1821.0	578	−0.02	−0.5	0.0462 ± 14	330.6 ± 4.2	17.2 ± 0.9	19.5 ± 0.3
4.1	23.06	1	448.0	42	0.40	14.2	0.0502 ± 29	325.4 ± 6.6	33.1 ± 5.2	19.7 ± 0.4
4.2	23.06	2	11310.0	158	0.06	24.2	0.0470 ± 5	383.6 ± 2.7	15.1 ± 4.6	16.8 ± 0.1
5.1	23.06	2	3967.0	652	0.21	8.0	0.0483 ± 10	398.5 ± 4.1	15.6 ± 0.8	16.1 ± 0.2
5.2	23.06	1	4092.0	169	0.17	24.7	0.0488 ± 5	103.8 ± 0.6	51.6 ± 5.4	61.7 ± 0.3
6.1	23.06	1	183.0	116	0.84	7.9	0.0548 ± 28	121.4 ± 3.4	56.6 ± 3.1	52.5 ± 1.5
7.1	23.06	1	655.0	858	1.06	5.2	0.0570 ± 14	111.9 ± 1.0	58.8 ± 1.2	56.7 ± 0.5
7.2	23.06	2	13625.0	438	0.10	21.5	0.0474 ± 7	370.2 ± 5.1	12.0 ± 2.4	17.4 ± 0.2
8.1	23.06	1	103.0	26	3.53	35.2	0.0797 ± 47	148.9 ± 4.3	69.3 ± 6.5	41.6 ± 1.2
8.2	23.06	2	6098.0	264	0.16	22.3	0.0478 ± 12	424.3 ± 3.4	12.3 ± 0.3	15.2 ± 0.1
9.1	23.06	1	381.0	239	0.01	0.2	0.0474 ± 20	99.9 ± 1.5	60.0 ± 2.3	64.2 ± 0.9
9.2	23.06	2	561.0	333	0.29	2.9	0.0497 ± 15	133.2 ± 1.8	50.2 ± 2.1	48.1 ± 0.6
10.1	23.06	1	1109.0	545	−0.01	−0.2	0.0472 ± 13	101.9 ± 0.9	65.0 ± 1.6	63.0 ± 0.5
10.2	23.09	2	7487.0	231	0.27	49.8	0.0489 ± 12	359.3 ± 3.8	11.3 ± 5.5	17.9 ± 0.2
11.1	23.06	1	60.0	78	0.69	3.7	0.0872 ± 13	4.8 ± 0.1	1261.5 ± 22.1	1221.0 ± 16.2
11.2	23.06	2	7070.0	979	0.11	5.5	0.0474 ± 8	357.1 ± 3.0	14.6 ± 0.7	18.0 ± 0.2
11.3	23.06	1	88.0	70	0.13	44.3	0.0815 ± 17	6.4 ± 0.1	1327.4 ± 33.0	918.2 ± 14.6
12.1	23.06	1	945.0	333	1.31	8.6	0.0487 ± 28	336.4 ± 5.2	36.1 ± 1.7	19.1 ± 0.3
12.2	23.06	2	14136.0	261	0.25	2.7	0.0476 ± 6	354.1 ± 4.5	9.6 ± 3.5	18.2 ± 0.2
13.1	23.06	1	938.0	33	0.55	88.1	0.0515 ± 26	353.3 ± 7.0	2.8 ± 10.3	18.1 ± 0.4
14.1	23.06	1	631.0	122	0.05	1.8	0.0482 ± 12	71.6 ± 0.6	83.0 ± 4.8	89.4 ± 0.7
14.2	23.09	2	13486.0	217	0.03	11.6	0.0467 ± 7	342.8 ± 3.6	19.0 ± 5.6	18.8 ± 0.2
15.1	23.06	1	1387.0	277	0.69	19.2	0.0528 ± 20	408.8 ± 6.0	16.6 ± 1.5	15.6 ± 0.2
16.1	23.06	1	328.0	12	1.83	105.0	0.0633 ± 78	507.7 ± 20.9		12.5 ± 0.5
16.2	23.06	2	7958.0	987	0.15	7.3	0.0478 ± 5	352.3 ± 3.2	17.0 ± 0.7	18.2 ± 0.2
17.1	23.06	1	3512.0	179	0.24	23.5	0.0495 ± 7	100.5 ± 0.6	61.0 ± 6.2	63.7 ± 0.4
18.1	23.06	1	841.0	33	0.07	9.4	0.0471 ± 21	353.5 ± 5.2	23.3 ± 7.8	18.2 ± 0.3
19.1	23.06	1	1365.0	569	0.38	5.2	0.0507 ± 11	115.2 ± 1.0	63.7 ± 2.0	55.5 ± 0.5
19.2	23.06	2	5176.0	736	0.14	6.5	0.0477 ± 7	381.3 ± 2.2	16.3 ± 0.8	16.9 ± 0.1
20.1	23.06	1	1308.0	568	0.15	2.6	0.0487 ± 10	101.9 ± 0.9	56.5 ± 1.7	62.9 ± 0.5
20.2	23.06	0	728.0	13	0.17	22.9	0.0479 ± 31	369.7 ± 5.4	38.5 ± 24.2	17.4 ± 0.3
20.3	23.09	2	9221.0	190	0.13	37.5	0.0476 ± 12	378.2 ± 4.1	14.4 ± 8.6	17.0 ± 0.2
21.1	23.09	2	12207.0	221	0.00	0.0	0.0462 ± 10	365.1 ± 2.5	21.1 ± 7.5	17.6 ± 0.1
22.1	23.09	2	15982.0	317	0.21	59.7	0.0483 ± 7	369.6 ± 3.0	8.4 ± 4.1	17.4 ± 0.1
22.2	23.09	1	398.0	456	0.41	2.4	0.0512 ± 25	99.6 ± 1.8	66.6 ± 1.7	64.4 ± 1.1
23.1	23.09	2	13641.0	3172	0.09	2.5	0.0473 ± 8	320.0 ± 3.1	20.8 ± 0.5	20.1 ± 0.2

%206c indicates the percentage of common ^{206}Pb correction in the total measured ^{206}Pb. %208c indicates the percentage of common ^{208}Pb correction in the total measured ^{208}Pb. Gaps in the $^{208}Pb/^{232}Th$ age column correspond to poorly resolved Th ages because of low Th content. All errors correpond to 1σ.

represents the age of crystallization of the Tangtse granite. Six data points define the older group with a weighted mean of 63.0 ± 0.8 Ma (2σ) and four data points show an age range decreasing from *c.* 60 to 40 Ma, suggesting these grains were affected by Pb loss. Two spots in the same zircon yielded much older ages at *c.* 1220 and 920 Ma (Table 1), suggesting involvement of older crustal rocks. One spot yielded *c.* 89 Ma (Table 1, Fig. 9a), which could either be an outlier or an inherited zircon from an older magmatic phase.

The younger group, comprising 25 analyses, mainly of zircon mantles but also of a few zircon cores (Fig. 9b, Table 1), yields a weighted mean age of 18.0 Ma, and a standard deviation of 1.4 Ma, and a standard error in the mean of 0.3 Ma (1σ). (spot 16.1 of 12.5 ± 0.5 Ma was considered an outlier and not included in this group.) The relatively high spread of ages (high standard

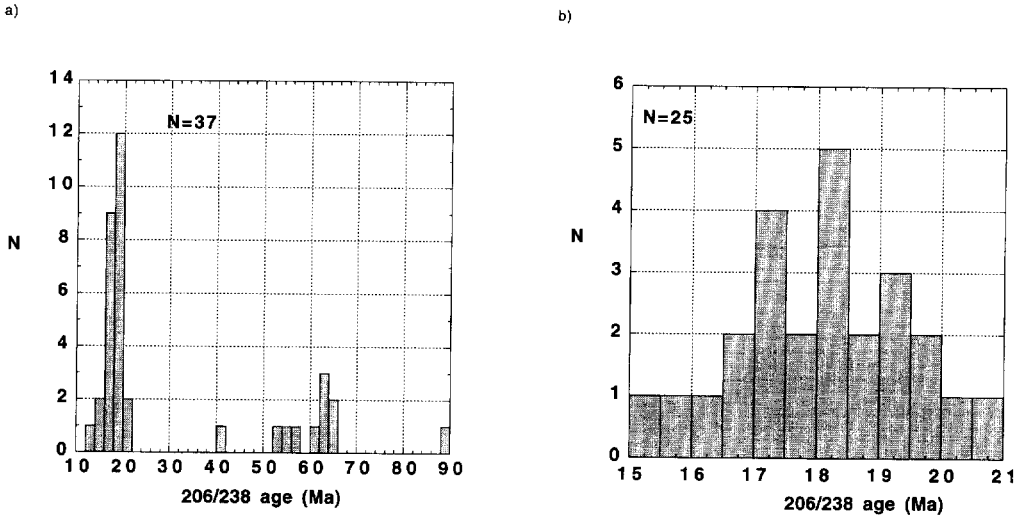

Fig. 9. Sample 215. (**a**) Stack histogram of the $^{206}Pb/^{238}U$ age distribution of 37 spots on zircons from the mylonitic Tangtse leucogranite determined using SHRIMP II. (**b**) Detailed histogram of the 25 young ages of mantles and cores.

deviation) compared with the relatively small individual errors (of the order of 0.3 Ma) suggests one of three possibilities: (a) the age spread is caused by either Pb loss or underestimation of U content in high-U zircons; (b) individual errors are underestimated; (c) the zircons have a true age spread.

A potential source for the high standard deviation could be the high U content of some analyses (up to 1.6% U), suggesting the possibility of calibration problems, but, in contrast to sample 022 (below), there is no clear relation between U content and age. Spots with relatively high Th contents yielded high-precision $^{208}Pb/^{232}Th$ ages. These were nearly identical within error to U/Pb ages (e.g. spots 1.1, 2.1, 3.1, 5.1, 11.2, 16.2, 19.2, 23.1 in Table 1), but with a consistent tendency towards lower values (spots 1.1, 3.1, 11.2, 16.2). This last observation suggests that either the high U content may in fact have caused small unwanted analytical effects or the U–Th–Pb system was opened after zircon crystallization. Either of these effects may explain the relatively large age spread, but neither was sufficiently important to have fundamentally changed the apparent age obtained.

The 18.0 ± 0.6 Ma (2σ) Tangtse granite is younger than the compositionally similar 21.0 ± 0.5 Baltoro granite (dated by conventional zircon U–Pb methods, (Parrish & Tirrul 1989)). The relatively short crystallization age difference between the two rocks and their similar geochemistry suggest they could have resulted from the same crustal melting event; such events typically last a few million years. The older 63.0 ± 0.8 Ma (2σ) cores are of clear igneous origin and are comparable in age with Rb–Sr ages on granitoids studied by Debon (1995) and Debon et al (1996) in the Hunza Karakoram in Pakistan.

Sample 022 has well-formed, prismatic zircons, 100–300 μm long. Under the microscope, these zircons can be divided into two groups: yellowish and clear transparent zircons, with some zircons showing yellowish cores overgrown by clear, transparent rims. Cathodoluminescence images show similar patterns to sample 215, with luminescent (low-U) cores with euhedral fine-scale oscillatory igneous zoning, truncated and overgrown by weakly luminescent (high-U) finely zoned prismatic mantles.

Dating defined two main age groups (Table 2 and Fig. 10): the yellowish zircons and cores represent an older phase with a weighted mean age of *c.* 106.3 ± 2.3 Ma (2σ), interpreted as the crystallization age of the orthogneiss. The transparent zircons and transparent rims represent a younger group ranging in age from 22 to 15 Ma, interpreted as dating zircon growth during partial melting of the orthogneiss.

U/Pb ages of the older group are confirmed by similar Th/Pb ages (Table 2). A few analyses, however, yielded U/Pb ages intermediate between the two main age groups suggesting Pb loss. Pb loss is confirmed by comparison to Th/Pb ages of these same spots, which are much

Table 2. *SHRIMP analys*

Spot	Date	Core (1) or rim (2)	(p
1.1	18.06	1	
1.2	18.06	2	
1.3	23.09	2	
2.1	18.06	1	1
2.2	23.09	1	1
3.1	18.06	2	
3.2	18.06	1	
4.1	18.06	2	
4.2	18.06	1	
5.1	18.06	2	
5.2	18.06	1	
6.1	18.06	2	
6.2	18.06	1	
7.1	18.06	1	9
8.1	18.06	2	1
8.2	18.06	1	
9.1	18.06	2	
9.2	18.09	1	
10.1	18.06	1	
11.1	18.06	2	
11.2	23.09	2	
11.3	23.09	1	
12.1	18.06	1	5
13.1	18.06	2	1
14.1	18.06		
15.1	18.06	1	
16.1	18.06	2	
16.2	18.06	1	6
17.1	18.06	1	
18.1	18.06	1	2
19.1	18.06	1	
19.2	23.09	2	
20.1	18.06	1	3
21.1	23.06	1	
22.1	23.06	1	3
23.1	23.06	1	3
23.2	23.09		6
24.1	23.06	1	
24.2	23.09	2	1
25.1	23.06	1	3
25.2	23.09	1	3
26.1	23.06	1	
26.2	23.09	2	
27.1	23.06	1	
28.1	23.06	2	
29.1	23.06	1	
30.1	23.06	1	
31.1	23.06	1	
32.1	23.06	1	
33.1	23.09	1	12
33.2	23.09	2	1

%206c indicates the perc
percentage of comm
correspond to poorly

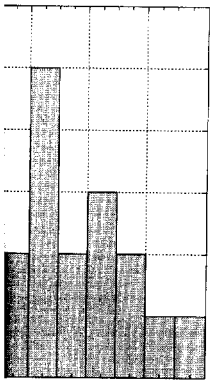

n zircons from the
of the 25 young ages of

ing event; such events
years. The older 63.0
f clear igneous origin
e with Rb–Sr ages on
on (1995) and Debon
Karakoram in Pakis-

ll-formed, prismatic
g. Under the micro-
be divided into two
r transparent zircons,
yellowish cores over-
t rims. Cathodolumi-
lar patterns to sample
w-U) cores with eu-
ory igneous zoning,
y weakly luminescent
natic mantles.
n age groups (Table 2
zircons and cores rep-
a weighted mean age
terpreted as the crys-
hogneiss. The trans-
rent rims represent a
ge from 22 to 15 Ma,
rcon growth during
gneiss.
oup are confirmed by
2). A few analyses,
ages intermediate
groups suggesting Pb
d by comparison to
pots, which are much

Table 2. *SHRIMP analyses of zircons from Pongong migmatite sample 022*

Spot	Date	Core (1) or rim (2)	U (ppm)	Th (ppm)	%206c	%208c	$^{207}Pb/^{206}Pb$	$^{238}U/^{206}Pb$	$^{208}Pb/^{232}Th$ age (1σ)	$^{206}Pb/^{238}U$ age (1σ)
1.1	18.06	1	101.8	101	3.29	19.7	0.0788 ± 46	55.3 ± 1.1	109.8 ± 5.3	111.7 ± 2.3
1.2	18.06	2	363.0	15	7.02	85.0	0.1117 ± 85	429.6 ± 13.3	29.8 ± 22.6	13.9 ± 0.5
1.3	23.09	2	265.3	17	3.23	85.8	0.0764 ± 77	464.0 ± 17.5	8.6 ± 13.5	13.4 ± 0.5
2.1	18.06	1	1107.9	18	2.03	86.0	0.0653 ± 33	374.3 ± 7.4	24.9 ± 27.1	16.8 ± 0.3
2.2	23.09	1	1274.5	19	0.60	89.9	0.0520 ± 23	407.2 ± 5.1	5.3 ± 19.9	15.8 ± 0.2
3.1	18.06	2	911.1	108	0.97	19.1	0.0558 ± 21	170.8 ± 3.1	92.0 ± 5.9	37.3 ± 0.7
3.2	18.06	1	134.3	96	4.74	31.6	0.920 ± 41	62.4 ± 2.0	102.3 ± 5.9	97.6 ± 3.1
4.1	18.06	2	233.0	14	14.44	86.5	0.1807 ± 271	401.1 ± 19.2	39.6 ± 51.3	13.7 ± 0.8
4.2	18.06	1	824.0	273	1.73	20.1	0.0634 ± 20	97.2 ± 0.9	95.7 ± 3.6	64.8 ± 0.6
5.1	18.06	2	283.4	16	14.33	114.7	0.1795 ± 313	635.9 ± 102.1		8.7 ± 1.4
5.2	18.06	1	312.7	227	1.24	11.0	0.0597 ± 27	58.4 ± 0.7	106.5 ± 4.6	108.1 ± 1.3
6.1	18.06	2	296.8	46	3.01	46.2	0.0751 ± 34	115.0 ± 2.4	87.3 ± 11.7	54.1 ± 1.1
6.2	18.06	1	113.7	118	3.13	18.7	0.0773 ± 48	55.9 ± 1.1	104.6 ± 6.4	110.7 ± 2.2
7.1	18.06	1	9384.1	31	0.22	103.3	0.0485 ± 8	302.6 ± 4.3		21.2 ± 0.3
8.1	18.06	2	1023.8	1777	0.39	1.6	0.0519 ± 8	56.8 ± 0.6	111.7 ± 1.3	112.1 ± 1.1
8.2	18.06	1	286.2	14	8.89	66.5	0.1291 ± 217	350.5 ± 26.5	111.9 ± 59.8	16.7 ± 1.3
9.1	18.06	2	280.6	127	2.18	24.3	0.0682 ± 36	63.6 ± 1.5	107.5 ± 8.2	98.4 ± 2.3
9.2	18.09	1	187.8	111	2.42	22.6	0.0706 ± 30	58.2 ± 1.0	108.5 ± 6.7	107.3 ± 1.9
10.1	18.06	1	391.7	262	1.17	10.5	0.0589 ± 24	60.6 ± 0.8	110.1 ± 4.5	104.3 ± 1.3
11.1	18.06	2	215.3	18	16.78	79.1	0.2025 ± 234	321.9 ± 32.7	71.4 ± 41.4	16.6 ± 1.8
11.2	23.09	2	210.1	8	36.72	4.0	0.3887 ± 92	63.8 ± 2.2		58.5 ± 2.3
11.3	23.09	1	97.7	60	35.86	3.3	0.3814 ± 100	33.9 ± 0.6		111.9 ± 2.9
12.1	18.06	1	5889.9	97	0.53	80.2	0.0514 ± 9	306.2 ± 4.7	12.0 ± 8.6	20.9 ± 0.3
13.1	18.06	2	1078.8	16	8.27	134.1	0.1232 ± 75	503.1 ± 16.7		11.7 ± 0.4
14.1	18.06		419.3	17	5.06	82.9	0.0935 ± 56	291.8 ± 7.4	39.9 ± 23.1	20.9 ± 0.5
15.1	18.06	1	292.9	189	1.93	16.9	0.0659 ± 26	61.8 ± 0.8	106.6 ± 4.1	101.4 ± 1.3
16.1	18.06	2	622.5	18	8.01	96.0	0.1209 ± 71	350.3 ± 12.3	14.4 ± 32.8	16.9 ± 0.6
16.2	18.06	1	6123.5	101	1.59	79.7	0.0612 ± 12	298.3 ± 3.0	37.5 ± 11.9	21.2 ± 0.2
17.1	18.06	1	826.2	304	0.64	10.0	0.0540 ± 12	61.6 ± 0.8	115.9 ± 3.8	103.2 ± 1.4
18.1	18.06	1	2187.8	37	2.02	97.7	0.0653 ± 24	316.7 ± 4.5	3.9 ± 21.5	19.9 ± 0.3
19.1	18.06	1	353.4	292	1.53	11.9	0.0624 ± 24	57.1 ± 0.9	107.5 ± 3.4	110.1 ± 1.7
19.2	23.09	2	729.1	142	1.05	13.1	0.0566 ± 33	155.6 ± 3.3	96.4 ± 5.8	40.9 ± 0.9
20.1	18.06	1	3758.0	134	0.94	68.5	0.0552 ± 12	319.0 ± 2.8	17.1 ± 5.0	20.0 ± 0.2
21.1	23.06	1	144.6	66	0.65	7.9	0.0540 ± 40	67.6 ± 1.5	112.3 ± 8.7	94.0 ± 2.2
22.1	23.06	1	3158.8	18	0.38	98.2	0.0499 ± 14	341.5 ± 5.0	1.6 ± 35.0	18.8 ± 0.3
23.1	23.06	1	3068.8	7	0.37	124.3	0.0498 ± 12	339.3 ± 2.9		18.9 ± 0.2
23.2	23.09		6421.8	47	0.17	88.5	0.0480 ± 10	338.4 ± 3.1	4.2 ± 21.5	19.5 ± 0.2
24.1	23.06	1	496.2	210	0.41	4.1	0.0512 ± 16	95.2 ± 1.5	108.3 ± 3.6	67.1 ± 1.0
24.2	23.09	2	1605.2	36	0.86	66.4	0.0544 ± 24	399.1 ± 7.7	20.2 ± 12.1	16.0 ± 0.3
25.1	23.06	1	3726.0	60	0.47	102.3	0.0508 ± 10	389.7 ± 4.1		16.4 ± 0.2
25.2	23.09	1	3356.1	64	0.22	60.6	0.0484 ± 12	391.0 ± 4.1	9.0 ± 7.9	16.6 ± 0.2
26.1	23.06	1	87.0	76	1.64	12.6	0.0633 ± 43	62.1 ± 1.4	98.4 ± 6.7	101.3 ± 2.3
26.2	23.09	2	730.4	20	1.24	70.4	0.0579 ± 37	390.9 ± 6.3	23.3 ± 17.8	16.3 ± 0.3
27.1	23.06	1	99.8	73	1.00	9.0	0.0575 ± 32	57.5 ± 1.4	110.9 ± 6.8	110.1 ± 2.7
28.1	23.06	2	936.0	52	0.94	25.2	0.0551 ± 31	310.2 ± 6.4	77.6 ± 10.2	20.6 ± 0.4
29.1	23.06	1	116.3	76	1.10	10.6	0.0583 ± 34	61.8 ± 1.2	104.3 ± 5.3	102.3 ± 2.0
30.1	23.06	1	118.1	109	1.15	8.4	0.0589 ± 25	57.7 ± 2.0	107.9 ± 5.9	109.5 ± 3.7
31.1	23.06	1	692.7	449	−0.02	−0.2	0.04800 ± 9	59.0 ± 0.4	109.8 ± 2.3	108.4 ± 0.7
32.1	23.06	1	358.5	268	1.34	10.4	0.0605 ± 22	62.0 ± 0.9	125.5 ± 4.2	101.8 ± 1.6
33.1	23.09	1	12674.0	311	0.14	28.7	0.04780 ± 8	307.6 ± 1.6	22.3 ± 5.2	22.5 ± 0.1
33.2	23.09	2	1902.8	30	0.20	35.0	0.0482 ± 16	388.6 ± 3.9	29.6 ± 14.1	16.6 ± 0.2

%206c indicates the percentage of common ^{206}Pb correction in the total measured ^{206}Pb. %208c indicates the percentage of common ^{208}Pb correction in the total measured ^{208}Pb. Gaps in the $^{208}Pb/^{232}Th$ age column correspond to poorly resolved Th ages because of low Th content. All errors correpond to 1σ.

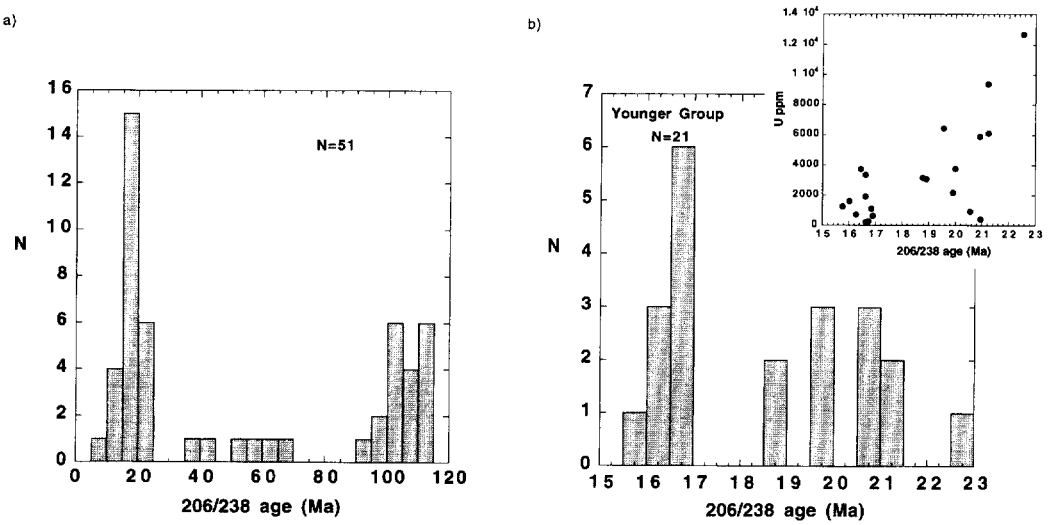

Fig. 10. Sample 022. (**a**) Stack histogram of the $^{206}Pb/^{238}U$ age distribution of 51 spots on zircons from the *in situ* granite of the Pangong migmatite. (**b**) Detailed histogram of the 26 spots analysed belonging to the young age group showing two distinct subgroups. Inset shows age plotted against U content, suggesting a positive relation between the two for spots with >6000 ppm of U.

less affected than U/Pb ages, yielding ages similar to those of unaffected zircons.

The younger age group, represented by 21 spot analyses, has a wide spread of ages that cannot be explained as resulting from a Gaussian distribution around a single mean age. The histogram in Fig. 10b suggests that this group may in fact represent two subgroups, one with weighted mean centred at 20.5 ± 0.7 Ma (2σ) and the other at 16.4 ± 0.2 Ma (2σ). A χ^2 test (a standard statistical test used to determine the likelihood that a group of measurements is derived from a parental distribution of measurements) for each subgroup suggests that whereas the younger subgroup is well described by a single age Gaussian distribution, the older subgroup is not and would need to be further divided. However, a closer look at the analyses of this subgroup (20.5 ± 0.7 Ma) shows that a few points have very high U content (up to 1.2%) and that the older ages within the subgroup are associated with the highest U content (insert in Fig. 10b; Table 2). This suggests that the age spread and the mean age of this subgroup might have been artificially raised by unwanted analytical effects (i.e. the instrument underestimated U content for high values).

Another point of concern regarding these two young subgroups is that their U/Pb ages could not be confirmed by Th/Pb ages, because of the large uncertainties owing to low Th content. A string of ungrouped younger ages (down to 8 Ma old) suggest that at least some zircons or parts of zircons may have undergone Pb loss. Thus, whereas high U seems to explain the spread towards older ages of the 20.6 Ma subgroup, Pb loss may explain the spread towards lower ages of the younger subgroup.

Despite these two effects, the strong grouping at *c.* 17 Ma and the group of low-U spots centred at *c.* 20 Ma still suggest two separate zircon growth phases. However, in view of the uncertainties, we choose to take the broader and safer interpretation that the partial melting of the 106 Ma orthogneiss occurred between 20 and 17 Ma, broadly contemporaneous with the age of crystallization of the intruding leucogranite (sample 215).

$^{40}Ar/^{39}Ar$ dating

The $^{40}Ar/^{39}Ar$ method of isotopic dating has been applied to micas from the Tangtse leucogranite sample dated above and to the Ladakh granodiorite at Taruk. This method, which relies on the decay of ^{40}K to ^{40}Ar and the subsequent retention of this argon in the mica lattice, commonly gives the age of cooling. Micas undergo closure to diffusion loss of ^{40}Ar from the lattice at about 300–350°C for cooling rates of tens of °C/Ma (± 100°C depending on a number of kinetic factors (Dodson & McClelland-Brown

T

Table 3. *$^{40}Ar/^{39}Ar$ step-he leucogranite, sample 128*

$^{40}Ar/^{39}Ar$	$^{37}Ar/^{39}Ar$ (10^{-3})
Sample 450 biotite, Taruk	
437.1	157.6
361.4	56.43
193.2	8.721
82.09	68.38
52.12	57.10
44.70	41.70
35.86	23.31
26.59	9.055
19.85	3.817
16.02	2.157
14.26	3.723
13.12	2.864
12.83	2.341
13.66	3.757
14.78	12.81
Sample 128 muscovite, Ta	
350.6	21.42
93.63	19.53
44.19	10.82
40.54	3.054
35.66	2.383
27.67	1.057
18.51	0.4508
16.61	0.1209
17.45	0.3936
18.87	0.5729
19.79	0.1314
19.57	0.0669
17.93	0.5363
16.44	0.9771
16.01	0.2069
16.45	0.8371
26.89	2.649

1985). Pure separates o
μm diameter) from the T
biotite (180–350 μm) fro
ite, SW of the Karakora
and subsequently step
furnace at progressively
(for analytical details, se
The muscovite yielded
plateau at 11.4 ± 0.1 Ma
yielded a similar plateau
3, Fig. 11). Despite the sm
temperatures between m

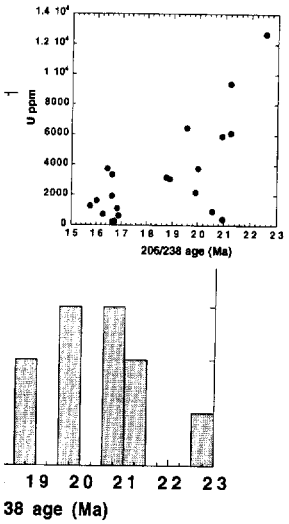

pots on zircons from the *in*
ysed belonging to the young
ent, suggesting a positive

ɔunger ages (down to 8 Ma
ıst some zircons or parts of
ıdergone Pb loss. Thus,
ns to explain the spread
the 20.6 Ma subgroup, Pb
pread towards lower ages
up.
ffects, the strong grouping
ıup of low-U spots centred
gest two separate zircon
ver, in view of the uncer-
ake the broader and safer
partial melting of the 106
ed between 20 and 17 Ma,
ɔous with the age of crys-
ling leucogranite (sample

d of isotopic dating has
cas from the Tangtse
lated above and to the
a: Taruk. This method,
ay of ^{40}K to ^{40}Ar and the
of this argon in the mica
the age of cooling. Micas
ısion loss of ^{40}Ar from the
50°C for cooling rates of
depending on a number
ion & McClelland-Brown

Table 3. *$^{40}Ar/^{39}Ar$ step-heating data for the Taruk granite biotite sample 450 and muscovite from the Tangtse leucogranite, sample 128*

$^{40}Ar/^{39}Ar$	$^{37}Ar/^{39}Ar$ (10^{-3})	$^{36}Ar/^{39}Ar$ (10^{-3})	^{39}Ar (10^{-16} mol)	Cumulative ^{39}Ar (%)	$\%^{40}Ar^*$	$^{40}Ar^*/^{39}Ar_K$	Calculated age (Ma) ± 1 SD	K/Ca
Sample 450 biotite, Taruk granite, ANU No. 95450, 100–420 μm, J = 0.0005449 ± 0.4%								
437.1	157.6	1367	0.1456	0.05	7.5	32.94	32.09 ± 27.75	3.3
361.4	56.43	1177	0.1561	0.10	3.6	13.06	12.80 ± 21.20	9.3
193.2	8.721	593.6	0.2517	0.18	9.1	17.51	17.13 ± 9.91	60.2
82.09	68.38	234.6	0.4276	0.32	15.1	12.38	12.13 ± 2.75	7.7
52.12	57.10	145.3	0.7582	0.57	16.9	8.817	8.65 ± 1.96	9.3
44.70	41.70	125.1	1.453	1.05	16.6	7.398	7.26 ± 1.11	12.6
35.86	23.31	82.89	2.782	1.97	30.7	11.01	10.79 ± 0.62	22.6
26.59	9.055	51.66	4.971	3.61	41.3	10.98	10.76 ± 0.34	58.1
19.85	3.817	27.93	8.307	6.35	56.6	11.23	11.01 ± 0.13	138
16.02	2.157	14.26	12.05	10.3	71.4	11.44	11.21 ± 0.15	244
14.26	3.723	7.748	16.12	15.7	81.4	11.61	11.38 ± 0.08	141
13.12	2.864	4.416	34.76	27.1	87.3	11.45	11.22 ± 0.05	184
12.83	2.341	3.022	33.65	38.2	90.2	11.58	11.35 ± 0.04	225
13.66	3.757	5.920	21.20	45.2	84.6	11.55	11.32 ± 0.07	140
14.78	12.81	9.728	166.0	100	78.1	11.54	11.31 ± 0.03	41.2
					Total	11.51	11.28 ± 0.11	101
Sample 128 muscovite, Tangste leucogranite, ANU No. 96216, 180–700 μm, J = 0.0004896 ± 0.4%								
350.6	21.42	1124	0.8712	0.2	5.1	17.96	15.79 ± 7.52	24.6
93.63	19.53	269.1	1.963	0.6	14.6	13.71	12.07 ± 1.19	27.0
44.19	10.82	102.5	3.517	1.4	30.5	13.49	11.88 ± 0.42	48.5
40.54	3.054	91.80	8.105	3.2	32.1	13.01	11.46 ± 0.29	172
35.66	2.383	75.71	17.70	7.2	36.2	12.89	11.35 ± 0.15	221
27.67	1.057	48.54	46.58	17.6	46.7	12.94	11.39 ± 0.07	498
18.51	0.4508	17.92	50.60	28.8	69.2	12.81	11.28 ± 0.05	1167
16.61	0.1209	11.63	64.60	43.2	76.9	12.77	11.24 ± 0.03	4348
17.45	0.3936	14.12	40.02	52.1	73.8	12.88	11.34 ± 0.04	1339
18.87	0.5729	18.81	29.08	58.6	68.4	12.91	11.36 ± 0.06	917
19.79	0.1314	22.38	26.55	64.5	64.5	12.77	11.25 ± 0.08	4000
19.57	0.0669	20.98	27.61	70.7	66.3	12.97	11.42 ± 0.08	7874
17.93	0.5363	15.69	31.10	77.6	71.9	12.89	11.35 ± 0.06	980
16.44	0.9771	10.65	33.00	85.0	78.4	12.89	11.35 ± 0.05	1901
16.01	0.2069	9.029	29.65	91.6	80.8	12.94	11.39 ± 0.08	2545
16.45	0.8371	10.12	21.24	96.3	79.4	13.05	11.49 ± 0.07	629
26.89	2.649	45.65	16.59	100	48.3	13.00	11.44 ± 0.11	199
					Total	12.90	11.36 ± 0.09	2134

1985). Pure separates of both muscovite (>700 μm diameter) from the Tangtse leucogranite and biotite (180–350 μm) from the Taruk granodiorite, SW of the Karakoram fault, were irradiated and subsequently step-heated in a vacuum furnace at progressively increasing temperatures (for analytical details, see Dunlap *et al.* (1995)). The muscovite yielded an age spectrum with a plateau at 11.4 ± 0.1 Ma and the Taruk biotite yielded a similar plateau at 11.3 ± 0.1 Ma (Table 3, Fig. 11). Despite the small difference in closure temperatures between muscovite and biotite, a conservative interpretation is that both samples cooled through 300–350°C and were at similar depths in the interval 11.4–11.3 Ma ago.

Geological offsets and timing of initiation of the Karakoram fault

Peltzer & Tapponnier (1988) proposed *c.* 1000 km of dextral motion along the Karakoram fault, but Searle (1996) demonstrated that these workers were linking up different granite belts that were never connected. The timing of

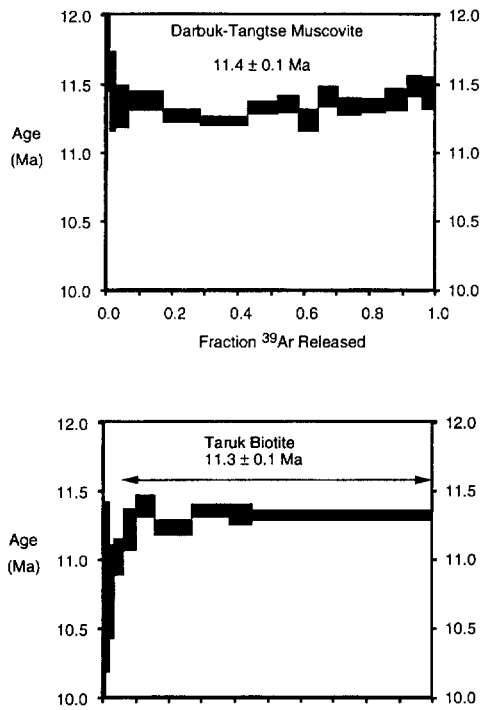

Fig. 11. Results from $^{40}Ar/^{39}Ar$ step-heating experiments on muscovites from the mylonitic Tangtse leucogranite (Karakoram terrane) and on biotites from the Taruk granodiorite (Ladakh batholith).

initiation of the Karakoram fault is crucial to determining if the fault can be related to the indentation of India into Asia and crustal extrusion of the thickened Tibetan plateau. If the fault was a major boundary of the eastwards extruding Tibetan crust, formed as a result of the India–Asia collision, then it would be expected that the fault initiated around the time of collision some 50 Ma ago. However, the Karakoram fault clearly cuts several geological features of widely ranging ages by a similar amount (*c.* 150 km). These include the late Cretaceous to early Eocene Ladakh granite batholith, the Miocene Baltoro and Tangtse granites of the Karakoram batholith, and the course of the Indus river (Searle 1996). Granites that were formed only *c.* 21 Ma ago in the Baltoro region (Parrish & Tirrul 1989) and *c.* 18.0 ± 0.6 Ma at Tangtse in northern Ladakh (this paper) have clearly been truncated by the later Karakoram fault. No two-mica garnet-bearing leucogranites occur SW of the Karakoram fault south of point (a) in Fig. 2. These granites are very distinct mineralogically and geochemically from the biotite + hornblende-bearing granodiorites of the Ladakh range to the south. North of the Baltoro granite plutons in northern Karakoram and Pamir there are no similar leucogranites to the Baltoro pluton exposed. Correlation of the Tangtse granite at point 'a'' in Fig. 2 with the Baltoro granite is therefore almost impossible to deny on geological evidence. The post-magmatic, dextral mylonitic S–C fabrics superimposed on the Tangtse granite along the southwestern strand of the Karakoram fault indicate that motion along the Karakoram fault in this area must have occurred after intrusion and crystallization of the Tangtse leucogranite.

We suggest that the fault was initiated soon after the intrusion of the Tangtse leucogranite, and dextral slip associated with movement along the fault imposed S–C fabrics on the granite in the greenschist facies. What is clear is that the fault was not initiated as a direct result of the Indian plate collision at *c.* 50 Ma; it is much more likely that it was initiated as a result of late Neogene crustal shortening in the Pamir indentor to the west (Searle 1996). This late-stage shortening in the Pamir has resulted in clockwise rotations in western Tibet, which are also reflected in the block rotations along the Karakoram fault (Armijo *et al.* 1989; Searle 1991).

Rates of dextral shear, cooling and exhumation

Maximum offsets of pre-Holocene geological features along the Karakoram fault are here determined to be 150 km right-lateral. Distinctive garnet–two-mica leucogranites of the Baltoro plutonic unit have been offset by this amount from the K12–Saltoro Kangri range in Pakistan to the Darbuk–Tangtse area in northern Ladakh. The Baltoro leucogranites and the Tangtse leucogranites have yielded early to mid-Miocene U–Pb zircon ages and have similar mineralogy and geochemistry, suggesting that they belong to the same plutonic unit and were subsequently separated by movement along the Karakoram fault. The average dextral strike-slip rate since 18.0 Ma was therefore 8.3 mm/a. $^{40}Ar/^{39}Ar$ results for the micas indicate that by 11.3 ± 0.1 Ma rocks on both sides of the Darbuk–Tangtse strand of the Karakoram fault were at similar temperatures, suggesting that uplift across the fault at this time was not rapid enough to induce significant thermal perturbations (e.g. differential cooling), and that thermal perturbation produced by rapid uplift since 18

Ma had largely relaxed. Exhumation of the deep crustal migmatites and leucogranites within the Karakoram fault zone must therefore have occurred between 18.0 and 11.3 Ma, when these rocks cooled from >700 to 350°C. The cooling rate from 18.0 to 11.3 Ma was therefore *c.* 50°C/Ma. We suggest that exhumation, erosion and unroofing of these migmatites and leucogranites within the fault zone occurred during this time; 11.3 Ma probably reflects the latest time at which the central part of the Karakoram fault changed from dominantly transpressional to dominantly strike-slip motion.

Along the entire Karakoram fault, maximum exhumation of deep crustal metamorphic and migmatitic rocks occurs in the Darbuk–Tangtse–Pangong area. To the NW and SE of this area, only upper-crustal shallower level rocks are exposed along the fault. At Tangtse, lineations consistently plunge at 20° towards the NW. Elsewhere in the Darbuk to Pangong Lake sector, lineation plunge varies from 0 to 30°. Given the measured 20° plunge in lineations along the Darbuk–Tangtse sector of the Karakoram fault, we can calculate the amount of uplift of the rock. At an average slip rate of 8.3 mm/a the dextral offset along the fault from 18.0 to 11.3 Ma would be *c.* 56 km. Assuming 56 km of dextral slip in 6.7 Ma at slip rates of 8.3 mm/a and a 20° plunge in lineations, the calculated uplift of the migmatites and leucogranite at Tangtse (tan 20° × 56) is 20.4 km at a mean rate of 3.0 mm/a.

Transpression and transtension

Although we argue here that the major phase of transpressive exhumation occurred in the Tangtse region between 18.0 and 11.3 Ma, there is evidence from along the Karakoram fault elsewhere of some later Pliocene–Quaternary transpression. Fission-track thermochronology from the K2 gneiss indicates that the K2–Gasherbrum range in north Pakistan has been uplifted by transpression within the last 5–7 Ma (Foster *et al.* 1994). The Pangong range in northeast Ladakh has also apparently been uplifted by transpression in Quaternary times, as shown by the morphology of hanging glaciers truncated by the fault scarp. At the same time, further SE along the Karakoram fault, the Gar basin opened by transtension (Armijo *et al.* 1989). Whereas the central part of the Karakoram fault accommodated most of the dextral slip, the northwest (Pamir) and southeast (Kailas) segments show dominantly dip-slip motion with Quaternary transtensional basins accumulating sediment eroded from the adjacent mountain ranges.

As India continued to penetrate northwards into Asia, Tibetan crust continued to thicken until the change from north–south compression to east–west extension. A series of ten N–S aligned graben systems in south Tibet are connected to NW–SE aligned dextral strike-slip faults, indicating that the two sets of faults may be temporally as well as spatially connected. Only two of the north–south normal faults have been dated by $^{40}Ar/^{39}Ar$ on muscovites, at *c.* 14 Ma in the Thakhola graben, northeast of Annapurna in north Nepal (Coleman & Hodges 1995) or *c.* 7–8 Ma in central Tibet (Harrison *et al.* 1992, 1995; Pan & Kidd 1992). We suggest that the timing of transpressional exhumation in the Tangtse sector of the Karakoram fault (18.0–11.3 Ma) immediately preceded initiation of the N–S normal faults in south Tibet and the beginning of E–W extension of the Tibetan plateau.

Tibet: to extrude or not to extrude – that is the question

Although strike-slip faults in and around the Tibetan plateau are some of the most impressive geological features, they do not show the very large amounts of offset that have previously been proposed (e.g. Peltzer & Tapponnier 1988). The Karakoram fault and the Altyn Tagh fault are undoubtedly extremely active faults today, cutting glacial features, truncating river terraces, changing the course of rivers and bounding rapidly uplifting mountain ranges. However, the estimation of Holocene slip rates cannot be determined with accuracy without precise dating of the offset geomorphological features, and present-day slip rates can certainly not be extrapolated back in the past beyond the Holocene. The pattern of strike-slip faults in Asia does suggest that some eastward motion of thickened Tibetan crust has occurred, but the amount of lateral extrusion can only be of the order of 100–200 km and not of the order of >1000 km demanded by the models of Tapponnier and co-workers. If it was of this order of magnitude the bounding strike-slip faults should show similar amounts of geological displacements.

Our work along the Karakoram fault, combined with detailed mapping and geochronology in the Pakistan sector (summarized by Searle (1991)) shows that, at least for the Karakoram fault, geological offsets since 18.0 Ma are no more than 150 km at mean slip rates of 8.3 mm/a, suggesting that crustal thickening of the Tibetan plateau was more important than lateral extrusion. Strain along the Karakoram fault was partitioned into predominantly dip-slip and

transtensional tectonics in the NW (Pamir) and SE (Gar to Mt Kailas) terminations and predominantly strike-slip with transpressionally uplifted mountain ranges in the central part of the fault in the K2–Gasherbrum range, Siachen glacier region and Tangtse area of northern Ladakh.

Conclusions

(1) The initiation of the Karakoram fault cannot have been older than 18.0 Ma, because it cuts and offsets granites of that age. The Karakoram fault cannot therefore be directly related to the 60–50 Ma India–Asia collision, which is much older. It is probably more likely to be a result of crustal shortening in the Pamir indentor and clockwise rotations of western Tibet.

(2) The maximum dextral offset along the Karakoram fault is 150 km based on offsets of the Baltoro-type granites in the Karakoram and the Ladakh batholith, and the offset course of the antecedent Indus river.

(3) Average dextral slip rates along the Karakoram fault since 18.0 Ma were 8.3 mm/a, approximately one-quarter of the proposed Holocene dextral slip rates proposed by Liu *et al.* (1992) and Avouac & Tapponnier (1993).

(4) Crustal melt garnet–two-mica leucogranites and migmatites were formed at 20–18 Ma at depths of >20 km in the Pangong range between the two strands of the Karakoram fault and were then exhumed by transpressional uplift from 18.0 to 11.3 Ma at rates of 3.0 mm/a.

(5) Maximum exhumation along the Karakoram fault occurred in the Tangtse area, where deep crustal rocks (Pangong metamorphic complex) are exposed within the fault zone. Northwest (Pamir and Shaksgam) and southeast (SW Tibet) of this area only upper-crustal rocks are exposed along the fault zone.

(6) $^{40}Ar/^{39}Ar$ dating of micas shows that by 11.3 ± 0.1 Ma ago temperatures of rocks on opposite sides of the Karakoram fault (but now at the surface 2 km apart) were similar, indicating an end of relative tectonic exhumation (uplift of the rock) by that time.

(7) Deformation was partitioned into a dominantly transpressional phase from 18.0 to 11.3 Ma, when exhumation of the Pangong migmatites and crustal melt granites within the Karakoram fault zone occurred, and a dominantly strike-slip phase starting from 11.3 Ma. The northwestern segment of the fault in the Pamir and the southeastern termination near Mt Kailas in southwest Tibet show dominantly dip-slip motion and Quaternary transtensional pull-apart basins.

(8) The relatively minor total offset along the Karakoram fault, combined with the age of initiation of dextral slip and the 8.3 mm/a slip rates suggest that the Karakoram fault has not accommodated the amount of eastward extrusion of the Tibetan plateau required by the extrusion model. The timings and amounts of exhumation, both in the Baltoro region and the Tangtse region, suggest that Asian crust was being actively thickened during the middle Miocene.

This work was supported by NERC Grant GT5/96/13/E to M. P. Searle. M. P. S. acknowledges with gratitude many discussions with P. Molnar, P. Tapponnier and J.-P. Avouac, even though they may not agree with our model. R. F. W. is very grateful to W. Compston for assistance with the SHRIMP analyses at the ANU and data reduction. R. F. W. and W. J. D. thank D. Green, R. Griffiths and I. McDougall for support. We thank the Australian Nuclear Science and Technology Organisation and the Australian Institute for Nuclear Science and Engineering for irradiations. We are extremely grateful to R. Parrish for a detailed review on the manuscript and discussions. We are also grateful to Fida Hussein Mitoo of Leh, D. Willis and J. Bradley for assistance in the field.

References

ARMIJO, R., TAPPONNIER, P. & HAN TONGLIN 1989. Late Cenozoic right-lateral strike-slip faulting across southern Tibet *Journal of Geophysical Research*, **94**, 2787–2838.

AVOUAC, J.-P. & TAPPONNIER, P. 1993. Kinematic model of active deformation in Central Asia. *Geophysical Research Letters*, **20**, 895–898.

BRUNEL, M., ARNAUD, N., TAPPONNIER, P., PAN, Y. & WANG, Y. 1994. Kongur Shan normal fault: type example of mountain building assisted by extension (Karakoram Fault, eastern Pamir). *Geology*, **22**, 707–710.

CERVENY, P. F., NAESER, C. W., KELEMEN, P. B. LIEBERMAN, J. E. & ZEITLER, P. K. 1989. Zircon fission-track ages from the Gasherbrum Diorite, Karakoram range, northern Pakistan. *Geology*, **17**, 1044–1048.

CLAOUÉ-LONG, J. C., COMPSTON, W., ROBERTS, J. & FANNING, C. M. 1995. Two Carboniferous ages: a comparison of SHRIMP zircon dating with conventional zircon ages and $^{40}Ar/^{39}Ar$ analysis. *In*: BERGGREN, W. A. *ET AL.* (eds) *Geochronology Time Scales and Global Stratigraphic Correlation.* Society for Sedimentary Geology Special Publication, **4**, 3–21.

——, JONES, P. J., ROBERTS, J. & MAXWELL, S. 1992. The numerical age of the Devonian–Carboniferous boundary. *Geological Magazine*, **129**, 281–291.

COLEMAN, M. & HODGES, K. 1995. Evidence for Tibetan plateau uplift before 14 Ma ago from a new minimum estimate for east–west extension. *Nature*, **374**, 49–52.

COMPSTON, W., WILLIAM
Geochronology of
73217 using a sensit
microprobe. *Journal*
B525–B534.

CRAWFORD, M. B. &
relations and geoc
(India–Asia) granitc
Karakoram, northe
206, 171–192.

DEBON, F. 1995. Incipien
plutonism: the Low
(Hunza Karakorum,
the Geological Socie

——, ZIMMERMAN, J. L.
Hunza granites (No
syn-collision bimod
taceous age. *Compt*
Sciences, **323**, 381–38

DODSON, M. H. & MCCLE
topic and palaeoma
cooling, uplift and
(ed.) *Geochronolo*
Geological Society
315–325.

DUNLAP, W. J., TEYSSIE
BALDWIN, S. 1995. T
ution of the intr
complex, central Au
1204.

FOSTER, D. A., GLEADOW
1994. Rapid Pliocer
koram (Pakistan), re
mochronology of th
19–22.

GILLESPIE, A. & MOLN
maximum advances
glaciers. *Reviews of*

HARRISON, T. M., COPEL
YIN 1992. Raising Ti

——, ——, —— & LOVE
the Nyainqentanghl
for uplift of southern
14, 658–676.

LIU, Q., AVOUAC, J.-P., T
1992. Holocene mo
part of the Karako
national Symposiun
KunLun Mountains,

MEYER, B., TAPPONNIER,
G., SHUNMIN, G. & Z
lateral movement
segment of the Alt
(China). *Geophysica*
29–44.

MOLNAR, P. & TAPPONNIE
of Asia, effects of a c
189, 419–426.

PAN, Y. & KIDD, W. S. F. 1
Zone: a late Miocen
southern Tibet platea

PARRISH, R. R. & TIRRU
Baltoro granite, nort
cations for zircon inh
systematics. *Geology*

COMPSTON, W., WILLIAMS, I. S. & MEYER, C. 1984. Geochronology of zircons from lunar breccia 73217 using a sensitive high mass-resolution ion microprobe. *Journal of Geophysical Research*, **89**, B525–B534.

CRAWFORD, M. B. & SEARLE, M. P. 1992. Field relations and geochemistry of pre-collisional (India–Asia) granitoid magmatism in the central Karakoram, northern Pakistan. *Tectonophysics*, **206**, 171–192.

DEBON, F. 1995. Incipient India–Eurasia collision and plutonism: the Lower Cenozoic Batura granites (Hunza Karakorum, North Pakistan). *Journal of the Geological Society, London*, **152**, 785–795.

——, ZIMMERMAN, J. L. & LEFORT, P. 1996. Upper Hunza granites (North Karakorum, Pakistan): a syn-collision bimodal plutonism of mid-Cretaceous age. *Comptes Rendus de l'Académie des Sciences*, **323**, 381–388.

DODSON, M. H. & MCCLELLAND-BROWN, E. 1985. Isotopic and palaeomagnetic evidence for rates of cooling, uplift and erosion. *In*: SNELLING, N. J. (ed.) *Geochronology and the Geologic Record* Geological Society, London, Memoirs, **10**, 315–325.

DUNLAP, W. J., TEYSSIER, C., MCDOUGALL, I. & BALDWIN, S. 1995. Thermal and structural evolution of the intracratonic Arltunga nappe complex, central Australia. *Tectonics*, **14**, 1182 – 1204.

FOSTER, D. A., GLEADOW, A. J. W. & MORTIMER, G. 1994. Rapid Pliocene exhumation in the Karakoram (Pakistan), revealed by fission track thermochronology of the K2 gneiss. *Geology*, **22**, 19–22.

GILLESPIE, A. & MOLNAR, P. 1995. Asynchronous maximum advances of mountain and continental glaciers. *Reviews of Geophysics*, **33**(3) 311–364.

HARRISON, T. M., COPELAND, P., KIDD, W. S. F. & AN YIN 1992. Raising Tibet. *Science*, **255**, 1663–1670.

——, ——, —— & LOVERA, O. M. 1995. Activation of the Nyainqentanghla Shear Zone: implications for uplift of southern Tibetan Plateau. *Tectonics*, **14**, 658–676.

LIU, Q., AVOUAC, J.-P., TAPPONNIER, P. & ZHANG, Q. 1992. Holocene movement along the southern part of the Karakoram Fault. *Abstracts, International Symposium on the Karakoram and KunLun Mountains*, Kashgar, China, 91.

MEYER, B., TAPPONNIER, P., GAUDEMER, Y., PELTZER, G., SHUNMIN, G. & ZHITAL, C. 1996. Rate of left-lateral movement along the easternmost segment of the Altyn Tagh fault, east of 96°E (China). *Geophysical Journal International*, **124**, 29–44.

MOLNAR, P. & TAPPONNIER, P. 1975. Cenozoic tectonics of Asia, effects of a continental collision. *Science*, **189**, 419–426.

PAN, Y. & KIDD, W. S. F. 1992. Nyainqentanghla Shear Zone: a late Miocene extensional detachment in southern Tibet plateau. *Geology*, **20**, 775–778.

PARRISH, R. R. & TIRRUL, R. 1989. U–Pb age of the Baltoro granite, northwest Himalaya, and implications for zircon inheritance and monazite U–Pb systematics. *Geology* **17**, 1076–1079.

PELTZER, G. & TAPPONNIER, P. 1988. Formation and evolution of strike-slip faults, rifts and basins during the India–Asia collision: an experimental approach. *Journal of Geophysical Research*, **93**, 15085–15117.

——, —— & ARMIJO, R. 1989. Magnitude of Late Quaternary left-lateral displacements along the north edge of Tibet. *Science*, **246**, 1285–1289.

REX, A. J., SEARLE, M. P., TIRRUL, R., CRAWFORD, M. B., PRIOR, D. J., REX, D. C. & BARNICOAT, A. 1988. The geochemical and tectonic evolution of the central Karakoram, North Pakistan. *Philosophical Transactions of the Royal Society*, London, **A326**, 229–255.

SCHÄRER, U., COPELAND, P., HARRISON, T. M. & SEARLE, M. P. 1990. Age, cooling history and origin of post-collisional leucogranites in the Karakoram batholith; a multi-system isotope study N. Pakistan. *Journal of Geology*, **98**, 233–251.

SEARLE, M. P. 1991. *Geology and Tectonics of the Karakoram Mountains.* John Wiley, Chichester.

—— 1996. Geological evidence against large scale pre-Holocene offsets along the Karakoram Fault: implications for the limited extrusion of the Tibetan Plateau. *Tectonics*, **15**, 171–186.

——, CRAWFORD, M. B. & REX, A. J. 1992. Field relations, geochemistry, origin and emplacement of the Baltoro granite, Central Karakoram. *Transactions of the Royal Society, Edinburgh, Earth Sciences*, **83**, 519–538.

——, PARRISH, R. R., TIRRUL, R. & REX, D. C. 1990. Age of crystallization and cooling of the K2 gneiss in the Baltoro Karakoram. *Journal of the Geological Society, London*, **147**, 603–606.

——, REX, A. J., TIRRUL, R., REX, D. C., BARNICOAT, A. & WINDLEY, B. F. 1989. Metamorphic, magmatic and tectonic evolution of the Central Karakoram in the Biafo–Baltoro–Hushe regions of North Pakistan. *Geological Society of America, Special Paper*, **232**, 47–73.

TAPPONNIER, P. & MOLNAR, P. 1976. Slip-line field theory and large scale continental tectonics. *Nature*, **264**, 319–324.

—— & —— 1977. Active faulting and tectonics in China. *Journal of Geophysical Research*, **82**, 2905–2930.

——, PELTZER, G. & ARMIJO, R. 1986. On the mechanics of the collision between India and Asia. *In*: COWARD, M. P. & RIES, A. C. (eds) *Collision Tectonics.* Geological Society, London, Special Publications, **19**, 115–157.

——, ——, LEDAIN, A. Y., ARMIJO, R. & COBBOLD, P. R. 1982. Propagating extrusion tectonics in Asia: new insights from simple experiments with plasticine. *Geology*, **10**, 611–616.

TAYLOR, S. R. & MCLENNAN, S. M. 1985. *The Continental Crust: It's Composition and Evolution.* Blackwell Scientific Publications, Oxford.

WEINBERG, R. F. & SEARLE, M. P. 1998. The Tangtse Injection Pangong Complex, Indian Karakoram: a case of pervasive granite flow through hot viscous crust. *Journal of the Geological Society, London,* in press.

WILLIAMS, I. S. & CLAESSON, S. 1987. Isotopic evidence for the Precambrian provenance and Caledonian

metamorphism of high grade paragneisses from the Seve Nappes, Scandinavian Caledonides, II, Ion microprobe zircon U–Th–Pb. *Contributions to Mineralogy and Petrology*, **97**, 205–217.

ZEITLER, P. K., SUTTER, J. F., WILLIAMS, I. S., ZARTMAN, R. & TAHIRKHELI, R. A. K. 1989. Geochronology and temperature history of the Nanga Parbat–Haramosh Massif, Pakistan. *Geological Society of America Special Publications*, **232**, 1–22.

Trans

MICHEL DE SAIN

[1]*CNRS – UMR55*
Sabatier, 38 rue des
[2]*Department of Ge*

[3]*Department of Ge*
55
[4]*CREGU, 54501 Va*

Abstract: Most
display strike-sli
structures in the
matics typifies m
tated strike-slip
almost normal t
by magmas beca
their ability to fo
component of m
ing the vertical p
tive feedback loo

We propose a
Strike-slip motio
margin-parallel
magma. The pa
caused by mecha
displacement fie
the upper-crusta

In oblique subduction, a
that some transcurrent n
within the magmatic arc
1986). Strike-slip faultin
edifice of many magmat
example, the central
Megard 1987), Sumatra
1988; Bellier & Sebrier 1
al. 1967; Lallemand &
Zealand (Cashman *et*
magmatic arcs where st
observed at the surface
crustal levels in erode
demonstrate strike-slip
tendency for magma
relations. These ancient
the Andes (Petford &
Cascades (Brown &
Batholith (Lund & Sne
Nevada (Busby-Spera &
Teyssier 1992). Strike-sl
with oblique subductio
obvious factors: (1) the
trend of the magmatic a

SAINT BLANQUAT, M., TIKO
and magmatic arcs. *In:* HOL
Transpressional and Transt
135, 327–340.